The Short-Term Cooling but Long-Term Global Warming Due to Biomass Burning

MARK Z. JACOBSON

Department of Civil and Environmental Engineering, Stanford University, Stanford, California

(Manuscript received 9 October 2003, in final form 6 February 2004)

ABSTRACT

Biomass burning releases gases (e.g., CO_2, CO, CH_4, NO_x, SO_2, C_2H_6, C_2H_4, C_3H_8, C_3H_6) and aerosol particle components (e.g., black carbon, organic matter, K^+, Na^+, Ca^{2+}, Mg^{2+}, NH_4^+, H^+, Cl^-, H_2SO_4, HSO_4^-, SO_4^{2-}, NO_3^-). To date, the global-scale climate response of controlling emission of these constituents together has not been examined. Here 10-yr global simulations of the climate response of biomass-burning aerosols and short-lived gases are coupled with numerical calculations of the long-term effect of controlling biomass-burning CO_2 and CH_4 to estimate the net effect of controlling burning over 100 yr. Whereas eliminating biomass-burning particles is calculated to warm temperatures in the short term, this warming may be more than offset after several decades by cooling due to eliminating long-lived CO_2, particularly from permanent deforestation. It is also shown analytically that biomass burning always results in CO_2 accumulation, even when regrowth fluxes equal emission fluxes and in the presence of fertilization. Further, because burning grassland and cropland yearly, as opposed to every several years, increases CO_2, biofuel burning, considered a ''renewable'' energy source, is only partially renewable, and biomass burning elevates CO_2 until it is stopped. Because CO_2 from biomass burning is considered recyclable and biomass particles are thought to cool climate, the Kyoto Protocol did not consider biomass-burning controls. If the results here, which apply to a range of scenarios but are subject to uncertainty, are correct, such control may slow global warming, contrary to common perception, and improve human health.

1. Introduction

Major anthropogenic sources of climate change are fossil-fuel combustion, biomass burning, biofuel burning, land-use change, and anthropogenically induced biological activity. Biomass burning is the burning of evergreen forests, deciduous forests, woodlands, grassland, and agricultural land, either to clear land for other use, to stimulate grass growth, for forest management, or as a ritual. Biomass burning, as defined here, does not include natural forest fires or biofuel burning. If biomass burning warms climate, though, it may feed back to enhance the frequency of natural fires (Stocks et al. 1998). Biofuel burning is the burning of biomass for electric power, home heating, and home cooking.

During biomass burning, aerosol particles, which are short-lived, and gases, which are short- and long-lived, are emitted. The major gas emitted during burning is carbon dioxide (CO_2). Other biomass-burning gases that can lead to climate change are methane (CH_4), nitrous oxide (N_2O), sulfur dioxide (SO_2), reactive organic gases (ROGs), and oxides of nitrogen (NO_x). The combination of ROGs and NO_x, for example, can produce ozone and particles, both of which affect temperatures.

Past studies of the effects of biomass burning on climate have focused on the radiative and optical properties of biomass-burning aerosol particles (e.g., Penner et al. 1992, 1998; Kaufman and Fraser 1997; Hobbs et al. 1997; Ross et al. 1998; Eck et al. 1998, 2001; Iacobellis et al. 1999; Grant et al. 1999; Christopher et al. 2000a,b; Kreidenweis et al. 2001; Zhang et al. 2001; Dubovik et al. 2002) and studies of temperatures in the vicinity of the smoke (e.g., Robock 1988; Tarasova et al. 1999). Such studies have generally concluded that biomass-burning particles tend to cool (Robock 1988) or neutralize (Tarasova et al. 1999) local surface temperatures or enhance negative forcing. Studies to date have not estimated the global-scale climate response of the combination of chemically reactive plus less reactive gases (e.g., CO_2, CO, CH_4, N_2O, NO_x, SO_2, ethene, propene, ethane, and propane) plus particle components (e.g., BC, OM, K^+, Na^+, Ca^{2+}, Mg^{2+}, NH_4^+, Cl^-, SO_4^{2-}, NO_3^-, and H_2O) from biomass burning. Houghton et al. (2001), for example, provide global radiative forcing estimates of a partial list of biomass-burning particles and, separately, a partial list of biomass-burning gases lumped with those of gases from other sources. It is not possible to extract, except crudely, a total gas plus aerosol direct plus indirect forcing of biomass burn-

Corresponding author address: Dr. Mark Z. Jacobson, Department of Civil and Environmental Engineering, Stanford University, Stanford, CA 94305-4020.
E-mail: jacobson@stanford.edu

ing from Houghton et al. (2001), nor has a verified relationship between total forcing and aerosol plus gas climate response been established. A study of the climate response to burning is important for evaluating biomass-burning reduction as a global-warming control strategy.

Here, the net climate response of controlling biomass burning over 100 yr is estimated by coupling numerical calculations of 100-yr temperature changes from controlling biomass-burning CO_2 and CH_4 in isolation with 10-yr global simulation temperature changes from controlling biomass-burning particles and gases, excluding the radiative effects of changes in CO_2 and CH_4. The 10-yr simulations were not run longer due to the substantial computer requirements [on three processors, each 10-yr simulation each took over 150 days of computer time (15 days yr^{-1}), which compares with 35 days yr^{-1} on one processor]. Section 2 of the paper describes the 100-yr projections, section 3 describes the model for the 10-yr global simulations, section 4 describes results from the 10-yr simulations including comparison with measurements for some parameters, and section 5 combines the 10- and 100-yr results.

2. One-hundred-year temperature change from controlling biomass CO_2 and CH_4

The temperature changes due to controlling biomass-burning CO_2 and CH_4 over 100 yr is estimated by solving ordinary differential equations for mixing ratio and combining the result with global three-dimensional equilibrium climate sensitivity calculations of the temperature response per unit mixing ratio. The mixing ratio of CO_2 with and without biomass burning is calculated by considering six major categories of emission: fossil-fuel combustion, biomass burning during permanent deforestation, biological decay during and after permanent deforestation, burning during temporary deforestation, biological decay during and after temporary deforestation, savannah/grassland burning, and agricultural burning. The calculation also considers regrowth of temporarily burned and decayed forest, of burned savannah/grassland, and of burned agriculture. It also considers the feedback of CO_2 to plant growth (CO_2 fertilization). Finally, it considers the loss of fossil-fuel and biomass-burning CO_2 due to all non-regrowth processes.

Biological-decay release of CO_2 during deforestation is considered here as part of biomass-burning emission. The purpose of most deforestation is to produce cropland and pastureland. Such deforestation is traditionally carried out by slashing trees, allowing them to dry for 2–3 months, then burning the slash and tree trunks prior to the rainy season. By this process, 20%–60% of the slash and dead leaves is burned (Kauffman et al. 1995; Carvalho et al. 1998, 2001). Most of the rest (70%–30% of the total) is decomposed by fungi, bacteria, and insects, and $<10\%$ of the total is removed to produce wood products (e.g., Houghton 1999). Since biological decay of the slash occurs following biomass burning, the CO_2 from such decay is considered here as part of CO_2 release associated with biomass burning.

Permanent and temporary deforestation are separated here since permanent deforestation results in a different net contribution to CO_2 than does deforestation followed by regrowth. Most slash-and-burn deforestation is permanent, but cropland and pastureland is sometimes abandoned, resulting in regrowth (the production of a secondary forest). Houghton et al. (2001) and Schlamadinger and Karjalainen (2000) predict that between 2008 and 2012, a deforestation flux of 1790 Tg CO_2–C yr^{-1} will be offset by reforestation plus afforestation (addition of new forest) fluxes of 200 to 580 Tg CO_2–C yr^{-1}. These numbers suggest that, to a first guess, about 10%–30% of deforestation is temporary and the rest is permanent.

Carbon dioxide emission from temporary forest burning, savannah/grassland burning, and agricultural burning is offset by regrowth. If an equal amount of emitted CO_2 were replaced immediately by regrowth, biomass burning would cause no net increase in atmospheric CO_2. Due to the time lag between burning and full regrowth, though, burning always causes a net atmospheric accumulation of CO_2, even when burning and regrowth rates equal one another. This is demonstrated here with a simple analytical solution. The full numerical solution accounting for this and other processes is discussed shortly.

Suppose a different parcel of forest is burned each year, emitting B_{ft} units of CO_2 each year. Suppose also that each parcel regrows exponentially at a rate corresponding to 70% regrowth after 25 yr (e.g., Houghton et al. 2000). Under such a condition, the exponential regrowth rate is $k_{\text{ft}} = 0.048\ 16\ \text{yr}^{-1}$, and the e-folding lifetime against regrowth is $\tau_{\text{ft}} = 1/k_{\text{ft}} = 20.76$ yr. In any given year t after burning of a given parcel, the quantity of CO_2 removed from the atmosphere to regrow the parcel is then $B_{\text{ft}}(1 - e^{-t/\tau_{\text{ft}}})$, and the rate of change of the mixing ratio (χ) of CO_2 due to continuous burning of different parcels and regrowth of all parcels is

$$\frac{d\chi(t)}{dt} = B_{\text{ft}} - B_{\text{ft}}(1 - e^{-t/\tau_{\text{ft}}}). \quad (1)$$

The analytical solution to this equation is

$$\chi(t) = \chi(0) + \tau_{\text{ft}}B_{\text{ft}}(1 - e^{-t/\tau_{\text{ft}}}). \quad (2)$$

Equation (2) predicts that, as t approaches infinity, the accumulation of CO_2 in the atmosphere is $\tau_{\text{ft}}B_{\text{ft}}$. This result is plotted graphically in Fig. 1a, which shows that yearly emission balances yearly uptake after about 100 yr, but the net CO_2 accumulation by that time is 21 times the annual emission rate.

Direct CO_2 emission from biomass burning (forest, savannah/grassland, and agricultural burning/shifting cultivation) has been estimated to range from 1320 to 4200 Tg CO_2–C yr^{-1} (Crutzen and Andreae 1990; Hao and Liu 1994; Liousse et al. 1996; Andreae and Merlet

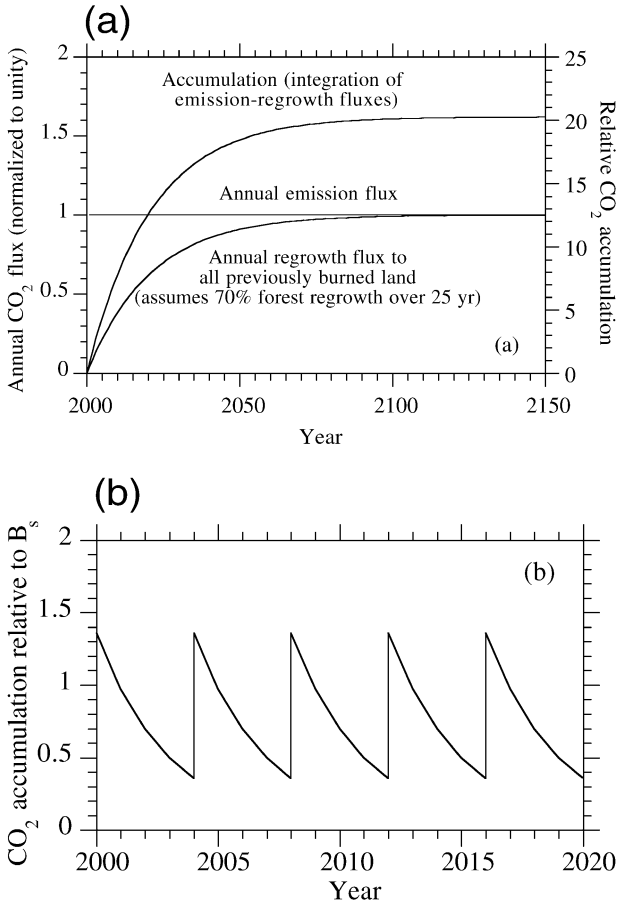

FIG. 1. (a) Accumulation in atmospheric CO_2 [from Eq. (1)] due to an annual one-unit emission flux ($B_{ft} = 1$) and an *e*-folding lifetime against regrowth of $\tau_{ft} = 20.76$ yr. The total accumulation at equilibrium is $\tau_{ft}B_{ft}$. (b) Yearly accumulation [from Eq. (3)] of atmospheric CO_2 from burning savannah every 4 yr instead of allowing the savannah to regrow completely before burning, assuming an annual one-unit emission flux ($B_s = 1$), $N_s = 4$ yr, and $\tau_s = 3$ yr. Increases are due to pulse burning every 4 yr. Decreases are due to regrowth.

2001). The most recent estimate is 2500 Tg CO_2–C yr^{-1} (Andreae and Merlet 2001). Here, it is assumed that the probable range of total CO_2–C emission from biomass burning is 1500–2700 Tg CO_2–C yr^{-1}. A higher upper limit would only strengthen the main conclusion of this study.

Of the total biomass burning, about one-third is from direct forest burning (Andreae and Merlet 2001; Bond et al. 2004). Andreae and Merlet estimate that CO_2 emission from forest burning is about 850 Tg CO_2–C yr^{-1}. Since burning consumes 20%–60% of deforested wood and assuming 10% is removed as wood products (discussed earlier), then 70%–30% (2975–425 Tg CO_2–C yr^{-1}) of the total wood is left as slash to decay. Although decay does not occur immediately, it can be shown mathematically that for a constant yearly deforestation rate and in steady state, the summed exponential decay rate in the current year among all previously deforested parcels equals the decay rate of one parcel, summed over all years. Thus, yearly CO_2 emission from deforestation burning plus decay may be 1275–3825 Tg CO_2–C yr^{-1}. Although 80% of this emission may be permanent, assume for illustration that 100% is temporary (regrows). From Eq. (2), the accumulation of CO_2 at equilibrium is 12–36 ppmv (with 1.096×10^{44} air molecules, 1 ppmv = 2184.82 Tg CO_2–C). In sum, even in the presence of regrowth and at equilibrium, biomass burning causes an accumulation of CO_2. This accumulation is offset somewhat by fertilization but is increased substantially because most deforestation today is permanent. These two factors are discussed shortly.

Carbon dioxide accumulates not only due to a time lag between burning and full regrowth but also due to the fact that parcels, such as agricultural land and savannah/grassland, burned yearly or every few years do not regrow to their full potential. For example, suppose the yearly emission rate from savannah burning is B_s. Also assume that the same parcel of savannah is burned every N_s years (and allowed to regrow in between), and the *e*-folding time for savannah regrowth is τ_s (years). Houghton (1999) estimates a grassland recovery time of about 10 yr in most locations (North America, Europe, Russia, China, Pacific developed, North Africa, Middle East), suggesting $\tau_s = 3$ yr (which gives 96.5% regrowth after 10 yr). In some locations (e.g., Latin America), the grassland regrowth time can be as low as 2 yr and in others (tropical Asia), up to 12 yr. Values of N_s may vary from 1 to 4 yr or more (Crutzen and Andreae 1990). Given that burned grassland often does not recover fully for several years, the upper limit may be more realistic in many cases. Since a savannah is generally burned before it is allowed to regrow completely, burning results in a time-dependent CO_2 accumulation in the atmosphere of

$$\Delta\chi(t) = \Delta\chi(0) + B_s^{\max}[1 - e^{-\mathrm{MOD}(t,N_s)/\tau_s}], \qquad (3)$$

where

$$B_s^{\max} = \frac{B_S}{1 - e^{-N_s/\tau_s}} \qquad (4)$$

is the emission rate due to burning the savannah when it is fully regrown. The first time the savannah is burned, $B_s^{\max}$ is emitted. Each subsequent burning, B_s is emitted and $B_s^{\max} - B_s$ stays in the atmosphere. Figure 1b illustrates Eq. (3) for a case where $B_s = 1$ unit of emission per year, $N_s = 4$ yr, and $\tau_s = 3$ yr. The figure shows that regular burning and incomplete regrowth causes a net increase in atmospheric CO_2 that varies in time between a low and high value. The accumulation is greater than Eq. (3) suggests if the original land use was more carbon intensive than the current use. For example, $B_s^{\max}$ is higher when a forest, woodland, or grassland is converted to farmland since farmland generally stores less biomass than do other land uses (e.g., Houghton 1999).

Equation (3) suggests that the regular burning of grassland or agricultural land rather than allowing roots

to grow deep and land to accumulate trees, brush, dead leaves, and dead wood, increases CO_2. This CO_2 buildup is similar to that which arises due to the frequent logging of forests instead of letting them accumulate biomass (Harmon et al. 1990) and differs only because the present process is due to biomass burning. The CO_2 buildup in the presence of annual burning also suggests that electric power from biofuels, considered renewable energy, is only partially renewable since biofuels (e.g., agricultural products) are taken from land before the land has regrown to its maximum potential.

For determining the 100-yr effect of controlling biomass-burning CO_2, it is assumed that burning rates are currently in equilibrium with regrowth rates with respect to temporary forest burning, savannah/grassland burning, and agricultural burning. Thus, the only future addition of CO_2 is due to permanent forest burning and decay. However, when burning is stopped, land is allowed to regrow to its maximum potential, removing accumulated CO_2 from the atmosphere. It is also assumed that biological decay occurs exponentially, and the current decay emission rate is the sum of the exponential decay rates in the current year from all previous years in which decay started. Thus, when burning is stopped, decay continues but decreases exponentially each year. Fertilization and its reverse are assumed to affect atmospheric CO_2 upon an increase and decrease, respectively, in CO_2. Under these assumptions, the ordinary differential equation describing the change in anthropogenic CO_2 in the presence of all forms of biomass burning considered is

$$\frac{d\chi(t)}{dt} = E_{\text{ff}} + B_{\text{fp}} + D_{\text{fp}} - \frac{\chi(t)}{\tau_{\text{all}}} - \frac{d\chi(t)}{dt}F \quad (5)$$

and that without biomass burning is

$$\frac{d\chi(t)}{dt} = E_{\text{ff}} + E_d(t) - R_{\text{ft}}(t) - R_s(t) - R_a(t) - \frac{\chi(t)}{\tau_{\text{all}}} - \frac{d\chi(t)}{dt}F, \quad (6)$$

where $\chi(t)$ is the anthropogenic mixing ratio of CO_2 (ppmv), E_{ff} is the fossil-fuel CO_2 emission rate (ppmv yr^{-1}), B_{fp} is the CO_2 emission rate due to permanent forest burning (ppmv yr^{-1}), D_{fp} is the CO_2 emission rate due to biological decay during permanent deforestation associated with burning (ppmv yr^{-1}) (and equals the equilibrium sum of exponential decay emission in the current year from all prior years), τ_{all} is the overall e-folding lifetime of CO_2 accounting for all non-regrowth and nonfertilization CO_2 removal processes, and F is the fertilization rate of CO_2 (ppmv CO_2 removed per ppmv change in CO_2 loading). In addition,

$$E_d(t) = (D_{\text{fp}} + D_{\text{ft}})e^{-t/\tau_d} \quad (7)$$

is the future emission from decay, where τ_d is the e-folding lifetime against decay [assumed to be 10 yr; Houghton (1999) estimates 2–33 yr for forests] and D_{ft} is the CO_2 emission rate (ppmv yr^{-1}) due to decay associated with temporary forest burning. Further,

$$R_{\text{ft}}(t) = (B_{\text{ft}} + D_{\text{ft}})e^{-t/\tau_{\text{ft}}}, \quad (8)$$

$$R_s(t) = B_s^{\max}[e^{-t/\tau_s} - e^{-(t+N_s)/\tau_s}], \quad \text{and} \quad (9)$$

$$R_a(t) = B_a^{\max}[e^{-t/\tau_a} - e^{-(t+N_a)/\tau_a}] \quad (10)$$

are regrowth rates of temporarily burned forests, savannah, and agricultural land, respectively, where τ_{ft}, τ_s, and τ_a are the e-folding times for regrowth of each vegetation type; N_s and N_a are the number of years between reburning the same savannah or agricultural parcel (the number of years between reburning a temporarily burned forest is assumed to be infinite); B_{ft} is the CO_2 emission rate (ppmv yr^{-1}) due to temporary forest burning; $B_s^{\max}$ was defined in Eq (4), and

$$B_a^{\max} = \frac{B_a}{1 - e^{-N_a/\tau_a}}, \quad (11)$$

where B_a is the yearly burning rate (ppmv yr^{-1}) of agricultural land.

Equations (5) and (6) are solved here numerically with the following respective solutions:

$$\chi(t) = \frac{\chi(t-h) + \dfrac{h}{1+F}(E_{\text{ff}} + B_{\text{fp}} + D_{\text{fp}})}{1 + \dfrac{h}{(1+F)\tau_{\text{all}}}}, \quad \text{and} \quad (12)$$

$$\chi(t) = \frac{\chi(t-h) + \dfrac{h}{1+F}\{E_{\text{ff}} + (D_{\text{fp}} + D_{\text{ft}})e^{-t/\tau_d} - (B_{\text{ft}} + D_{\text{ft}})e^{-t/\tau_{\text{ft}}} - B_s^{\max}[e^{-t/\tau_s} - e^{-(t+N_s)}/\tau_s] - B_a^{\max}[e^{-t/\tau_a} - e^{-(t+N_a)/\tau_a}]\}}{1 + \dfrac{h}{(1+F)\tau_{\text{all}}}}, \quad (13)$$

where h is the time step size (yr). The initial anthropogenic mixing ratio of CO_2 is assumed to be 95 ppmv, equal to the total mixing ratio in 2000 (370 ppmv) minus the preindustrial mixing ratio in 1750 (about 275 ppmv). The background mixing ratio of CO_2 (275 ppmv) is assumed to be in equilibrium with its natural emission and loss rates. The overall lifetime of CO_2 used here is assumed to range from τ_{all} = 30–95 yr, which encompasses the range required for observed mixing ratios to be consistent with emission rates from 1960–2000 (Jacobson 2004). From Eq. (12), CO_2 accumulation due to permanent forest burning, like fossil-fuel burning, is always limited by loss of CO_2 to non-regrowth processes.

The global fossil-fuel emission rate of CO_2 in 2000 (and from 1995–2000) was near E_{ff} = 3.02 ppmv yr^{-1} (6600 Tg CO_2–C yr^{-1}) (Marland et al. 2003). The total biomass-burning emission ($B_{tot} = B_{fp} + B_{ft} + B_s + B_a$) for Eqs. (12) and (13) is assumed to range from 0.687 to 1.24 ppmv yr^{-1} (1500–2700 Tg CO_2–C yr^{-1}; see discussion above). Of the total, 32.1% is assumed to be due to forest burning ($B_{fp} + B_{ft}$), 59.5% is assumed to be due to savannah/grassland burning (B_s), and 8.4% is assumed to be due to agricultural burning (B_a) (Andreae and Merlet 2001). Of the total forest burning, 80% is assumed to be permanent forest burning (see discussion above). Two sets of CO_2 emission rates due to biological decay are considered: $D_{fp} = B_{fp}$, $D_{ft} = B_{ft}$ and $D_{fp} = 3\,B_{fp}$, $D_{ft} = 3\,B_{ft}$. These rates account for the fact that 20%–60% of deforested land is burned while 70%–30% decays. It is further assumed that savannah lands are burned every 4 yr and agricultural lands are burned every year (N_s = 4 yr, N_a = 1 yr). Finally, it is assumed that τ_{ft} = 20.76 yr, and $\tau_s = \tau_a$ = 5 yr. This last assumption implies that, if left unburned, savannah/grassland and cropland might accumulate brush and sparse trees in addition to just fully regrown grass.

Finally, the fertilization rate is calculated from results of Poorter (1993), who found that doubling CO_2 from a range of 300–360 to 600–720 ppmv increased the average mass of 156 plant species by 37%. The extent to which fertilization increases the rate of tree growth only as opposed to also increasing long-term carbon storage is uncertain (Bolin and Sukumar 2000, p. 39). Nevertheless, assuming a 37% vegetation mass increase upon a doubling of CO_2 from 360 to 720 ppmv and assuming 470 Tg C currently stored in vegetation globally (Bolin and Sukumar 2000, p. 31), gives F = 0.37 × 470 Tg/(360 ppmv × 2.184 82 Tg/ppmv) = 0.22. This coefficient implies that, for every ppmv increase (decrease) in atmospheric CO_2, one-fifth is removed (added) by fertilization. Since fertilization increases the amount of biomass on some land that will be deforested, fertilization also increases biomass burning and biological decay, but that small feedback is not treated here.

Figures 2a,b show the projected changes in total CO_2 [background 275 ppmv plus time-dependent anthropogenic $\chi(t)$, starting at 95 ppmv] due to biomass burning and its elimination [Eqs. (12) and (13)], from 2000–2100. The two figures shown represent low and high estimates of the effects of controlling biomass-burning CO_2. The low estimate (Fig. 2a) assumes τ_{all} = 30 yr, B_{tot} = 0.687 ppmv yr^{-1} (1500 Tg CO_2–C yr^{-1}), $D_{fp} = B_{fp}$, and $D_{ft} = B_{ft}$. The high estimate (Fig. 2b) assumes τ_{all} = 95 yr, B_{tot} = 1.24 ppmv yr^{-1} (2700 Tg CO_2–C yr^{-1}), $D_{fp} = 3\,B_{fp}$, and $D_{ft} = 3\,B_{ft}$.

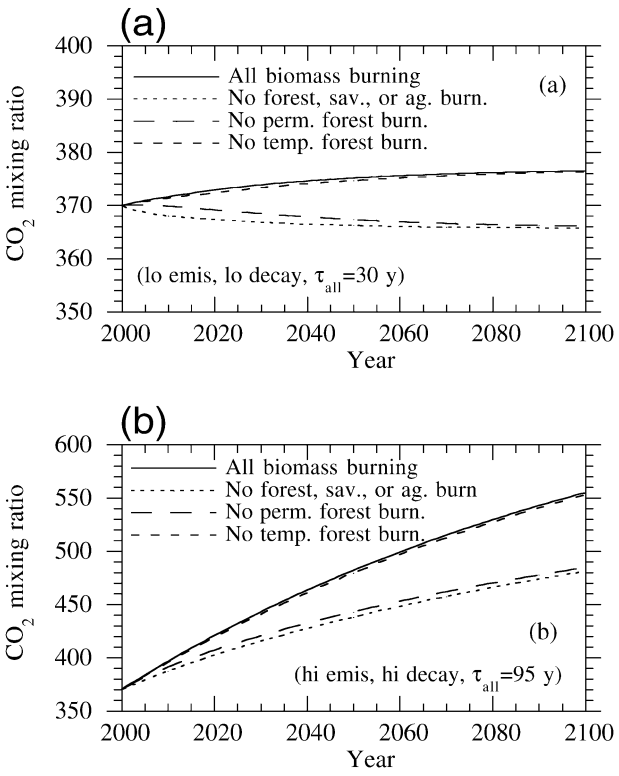

FIG. 2. (a) CO_2 mixing ratio versus time for four cases: with all biomass-burning emission ("All biomass burning") [Eq. (12)], with no biomass-burning emission ("No forest, sav., or ag. burn") [Eq. (13)], with all biomass burning except permanent forest burning ("No perm. forest burn.") [Eq. (13) with B_{ft}, D_{ft}, B_s^{max}, and B_a^{max} = 0], and with all biomass burning except temporary forest burning ("No temp. forest burn.") [Eq. (12) with $D_{ft}e^{-t/\tau_d} - (B_{ft} + D_{ft})e^{-t/\tau_{ft}}$ added to the argument on the right side of the numerator]. Fossil-fuel emissions were accounted for in all cases, τ_{all} = 30 yr, B_{tot} = 0.687 ppmv yr^{-1} (1500 Tg CO_2–C yr^{-1}), $D_{fp} = B_{fp}$, and $D_{ft} = B_{ft}$. Other conditions are described in the text. (b) Same as (a), except τ_{all} = 95 yr, B_{tot} = 1.24 ppmv yr^{-1} (2700 Tg CO_2–C yr^{-1}), $D_{fp} = 3B_{fp}$, and $D_{ft} = 3B_{ft}$.

Of the total biomass-burning CO_2 reduction after 100 yr in Figs. 2a,b, 94%–97% was due to eliminating permanent forest burning/decay, 2%–4% was due to eliminating temporary forest burning/decay, 0.8%–2% was due to eliminating savannah burning, and 0.1%–0.3% was due to eliminating agricultural burning. Thus, removing permanent forest burning decreased CO_2 far more than did removing other burning processes. Since CO_2 accumulation due to temporary forest burning was limited by regrowth, controlling temporary burning reduced CO_2 to a lesser extent than did controlling per-

manent burning. In fact, the reduction in CO_2 due to eliminating processes in which regrowth occurred diminished over time. For example, after 25 yr, eliminating savannah burning was responsible for about 11% of the total CO_2 reduction, but after 100 yr, it was responsible for only 0.8%–2% of the reduction. The reason is that the equilibrium CO_2 accumulated (e.g., Fig. 1) due to burning/regrowth diminishes over time due to non-regrowth removal (governed by τ_{all}). Such removal also affects permanent burning. However, since permanent burning produces a steady-state quantity of CO_2, $\chi(t) = \tau_{all}(B_{fp} + D_{fp})$ [found by setting $E_{ff} = 0$ and setting the derivatives in Eq. (5) to zero], its removal reduces only a steady-state quantity as well.

The time-dependent temperature response to controlling biomass-burning CO_2 emissions from 2000–2100 is projected here as

$$\Delta T(t) = \Delta\chi(t)\Delta T_{eq}/\Delta\chi_{eq}, \quad (14)$$

where $\Delta\chi(t)$ is the change in the time-dependent mixing ratio of CO_2 due to eliminating all biomass burning [Eq. (12) minus Eq. (13), the result of which is shown in Figs. 2a,b], and $\Delta T_{eq}/\Delta\chi_{eq}$ is the ''equilibrium climate sensitivity'' of CO_2 from Jacobson (2002a). This sensitivity was calculated by running a pair of global simulations, one in which the total CO_2 mixing ratio was included at current levels and a second in which it was included at preindustrial levels. The temperature difference between the two simulations divided by the mixing ratio difference is the equilibrium climate sensitivity, calculated as $\Delta T_{eq}/\Delta\chi_{eq} = -0.9$ K/95 ppmv in that case. Since there is uncertainty in the equilibrium climate sensitivity (because of the equilibrium assumption, the neglect of feedbacks from biomass burning to the carbon cycle buffering in the oceans and biosphere, etc.), and to ensure the climate response of removing CO_2 was not underestimated, a second equilibrium climate response of $\Delta T_{eq}/\Delta\chi_{eq} = -1.3$ K/95 ppmv, representing an extreme upper bound, is also considered here. Figure 3a shows ΔT_t for four cases: the two equilibrium climate sensitivities applied to each the low and high mixing ratio differences from Figs. 2a,b. The figure projects that eliminating CO_2 alone from biomass burning could decrease temperatures by -0.15 to -1 K. Much of this decrease in the latter case is due to the decrease of future CO_2 accumulation that would occur if permanent forest burning were stopped.

A simpler approach is used to estimate the change in mixing ratio due to eliminating biomass-burning CH_4: Eq. (5) is integrated after setting $F = 0$ and $D_{fp} = 0$ and replacing B_{fp} with B_{CH_4}, τ_{all} with τ_{all,CH_4}, and E_{ff} with E_{ff,CH_4}, then taking the difference of the solution when $B_{CH_4} = 0$. The result is

$$\Delta\chi_{CH_4}(t) = \tau_{CH_4}B_{CH_4}(1 - e^{-t/\tau_{CH_4}}), \quad (15)$$

where $B_{CH_4} = 0.0096$ ppmv yr^{-1} (21 Tg CH_4–C yr^{-1}), which is the emission rate of CH_4 from forest, savannah/grassland, and agricultural burning calculated in Andreae and Merlet (2001), and τ_{all,CH_4} is assumed to be a standard value of 10 yr. Figure 3b shows the temperature change, calculated when Eqs. (15) and (14) are coupled. The equilibrium climate sensitivity of CH_4 used is $\Delta T_{eq}/\Delta\chi_{eq} = 0.27$ K/1 ppmv (Jacobson 2002a).

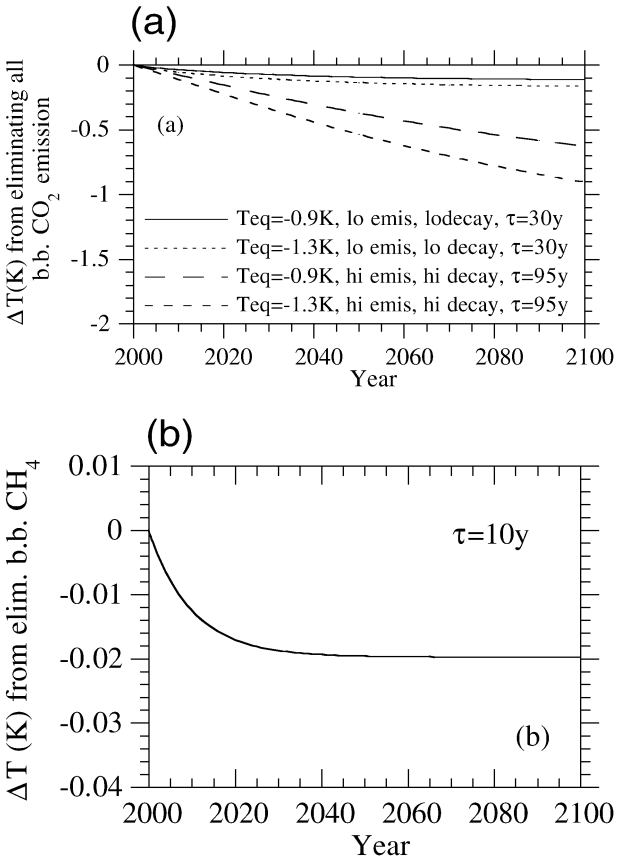

FIG. 3. (a) Change in temperature over 100 yr due to eliminating all biomass-burning CO_2 emission in isolation, calculated from Eq. (14), where $\Delta\chi(t)$ is determined by subtracting Eq. (13) from Eq. (12). The four cases shown account for two equilibrium climate sensitivities, each applied to the full-removal cases of Figs. 2a,b. (b) Change in temperature over 100 yr due to eliminating all biomass-burning CH_4 emission in isolation, calculated from Eqs. (14) and (15). Additional conditions are described in the text.

3. Description of the 10-yr global simulations

The model used for the 10-yr climate-response simulations was GATOR-GCMOM Jacobson 1997; 2001a,b,c; 2002a,b). It treated time-dependent gas, aerosol, radiative, meteorological, cloud, transport, and ocean processes over a 4°S–N × 5°W–E grid with 39 sigma pressure layers up to 0.425 hPa (~55 km) including 23 tropospheric layers and 3 layers below 1 km.

The model version used was the same as in Jacobson (2002a). The model treated at least 12 feedbacks of aerosol particles to climate, described therein. Gas processes included emission, gas chemistry, gas–aerosol–surface chemistry, advection, turbulence, cloud con-

vection of gases, nucleation, condensation, dissolution into aerosols, clouds, and precipitation, washout, and dry deposition. Predicted meteorology was initialized with National Centers for Environmental Prediction reanalysis fields (NCEP 2002). Aerosol size and composition and gas fields were initialized as described in Jacobson (2001b,c).

The model treated particle number concentration and mole concentrations of H_2O(aq), H^+, NH_4^+, Na^+, H_2SO_4(aq), HSO_4^-, SO_4^{2-}, NO_3^-, Cl^-, BC, organic matter [OM = organic carbon (OC) + functional groups], and soil dust in each of 17 size bins in each grid cell. Due to computational constraints, only one internally mixed size distribution was considered. Because each size bin was independent from others, some bins at some locations were relatively externally mixed, whereas others were relatively internally mixed. Treating a single instead of multiple size distributions may overestimate aerosol direct forcing by 20% (Jacobson 2001d), but the effect on temperature is less certain.

Aerosol and gas emissions are described in detail in Jacobson (2002a). With respect to biomass burning, monthly gridded emission rates of the particulate components, BC, OM, K^+, Na^+, Ca^{2+}, Mg^{2+}, NH_4^+, Cl^-, SO_4^{2-}, and NO_3^-, and the gases, CO_2, CO, CH_4, N_2O, NO_x, SO_2, ethene, propene, ethane, and propane, were obtained by multiplying monthly gridded biomass-burning BC emissions from Cooke and Wilson (1996) by the ratio of the mean biomass-burning emission factor for each gas or particle component to that of BC (Ferek et al. 1998). The ions K^+, Ca^{2+}, and Mg^{2+} were not carried in the simulations, but their mole-equivalent emissions were added to those of Na^+. The global biomass-burning BC emissions from Cooke and Wilson was 6 Tg C yr^{-1}. The uncertainty given by these authors is about a factor of 2, and this uncertainty is extended here to other species, whose emission rates are scaled from those of BC. Andreae and Merlet (2001) calculated a BC emission rate from nonbiofuels biomass burning of 3.1 Tg C yr^{-1}. To address some of the uncertainty in the Cooke and Wilson inventory and to account for the new results, the baseline BC inventory used here was reduced here by 25% to 4.5 Tg BC–C yr^{-1}. In addition, a sensitivity of the climate response (section 4) to a lower BC emission rate that encompasses that of Andreae and Merlet (2001) was performed. For that sensitivity, all other biomass gas and particle components were reduced proportionately as well.

Biomass-burning particles were emitted assuming three lognormal modes: nucleation, accumulation, and coarse modes with peak number diameters of 10, 100, and 1500 nm, respectively. Data from Reid and Hobbs (1998) suggest that smoke number emissions in the accumulation mode dominate those in the nucleation mode.

Baseline biomass-burning CO_2 and CH_4 emissions from the same technique were 2700 Tg CO_2–C yr^{-1} and 21 Tg CH_4–C yr^{-1} (4.5 Tg BC–C yr^{-1} multiplied by 900 g CO_2–C/kg^{-1} C burned 7 g CH_4–C kg^{-1} C burned, respectively, and divided by 1.5 g BC–C kg^{-1} C burned (Ferek et al 1998), consistent with the upper estimate of CO_2 and the only estimate of CH_4 emission discussed in section 2. Nonbiomass-burning anthropogenic CO_2 and CH_4 emissions globally were 6600 Tg CO_2–C yr^{-1} (Marland et al. 2003) and 268 Tg CH_4–C yr^{-1} (Stern and Kaufman 1998).

Other size- and composition-resolved aerosol processes included homogeneous nucleation, coagulation, growth by condensation and dissolution, water uptake, liquid and solid equilibrium chemistry, irreversible aqueous chemistry, advection, turbulence, cloud convection of aerosols, dry deposition, settling, rainout, and washout. Condensational growth was treated for H_2SO_4 and OM; dissolutional growth was treated for HCl, HNO_3, and NH_3.

Jacobson (2003) described the cloud scheme. Briefly, cumulus and stratus parameterizations were used to determine water available for cloud processes. The cumulus parameterization (Ding and Randall 1998) produced multiple subgrid clouds per column, each with a different cloud base and top (about 500 base and top combinations were possible in each column although 1–10 typically formed). Water and energy transport in each cloud was solved with a mass-flux convection scheme. Such a scheme can be used for tracers, as done by Mari et al. (2000), but the mass-flux scheme here is explicit, so it can produce negative concentrations in the presence of strong gradients. Instead, a positive–definite, stable convective plume transport scheme was used to transport bin-resolved aerosol components and gases in each subgrid cloud. Following transport, liquid and ice from the cumulus parameterization were evaporated/sublimated, then regrown onto size-resolved aerosols transported to that layer. Because aerosols were transported vertically with cloud water, their activation was consistent with their activation in a rising plume. Following growth, size-resolved processes treated were coagulation (liquid–liquid, ice–ice, and ice–liquid), large drop breakup, evaporative cooling during drop settling, evaporative freezing (freezing during drop cooling), heterogeneous and homogeneous freezing, contact freezing, melting, evaporation, sublimation release of aerosol cores upon evaporation/sublimation, coagulation with interstitial aerosols, irreversible aqueous chemistry, and lightning generation from size-resolved coagulation among ice hydrometeors.

Radiation processes included UV, visible, solar IR, and thermal IR radiative interactions with gases, size-/composition-resolved aerosols, and size-/composition-resolved hydrometeors. Radiation affected photolysis and heating. The dynamical portion solved for wind, temperature, pressure, and turbulence.

Sea surface temperature, ocean current velocities, and ocean mixed layer depths were predicted with a 2D potential enstrophy and mass-conserving shallow-water equation mixed layer module forced by wind stress (G.

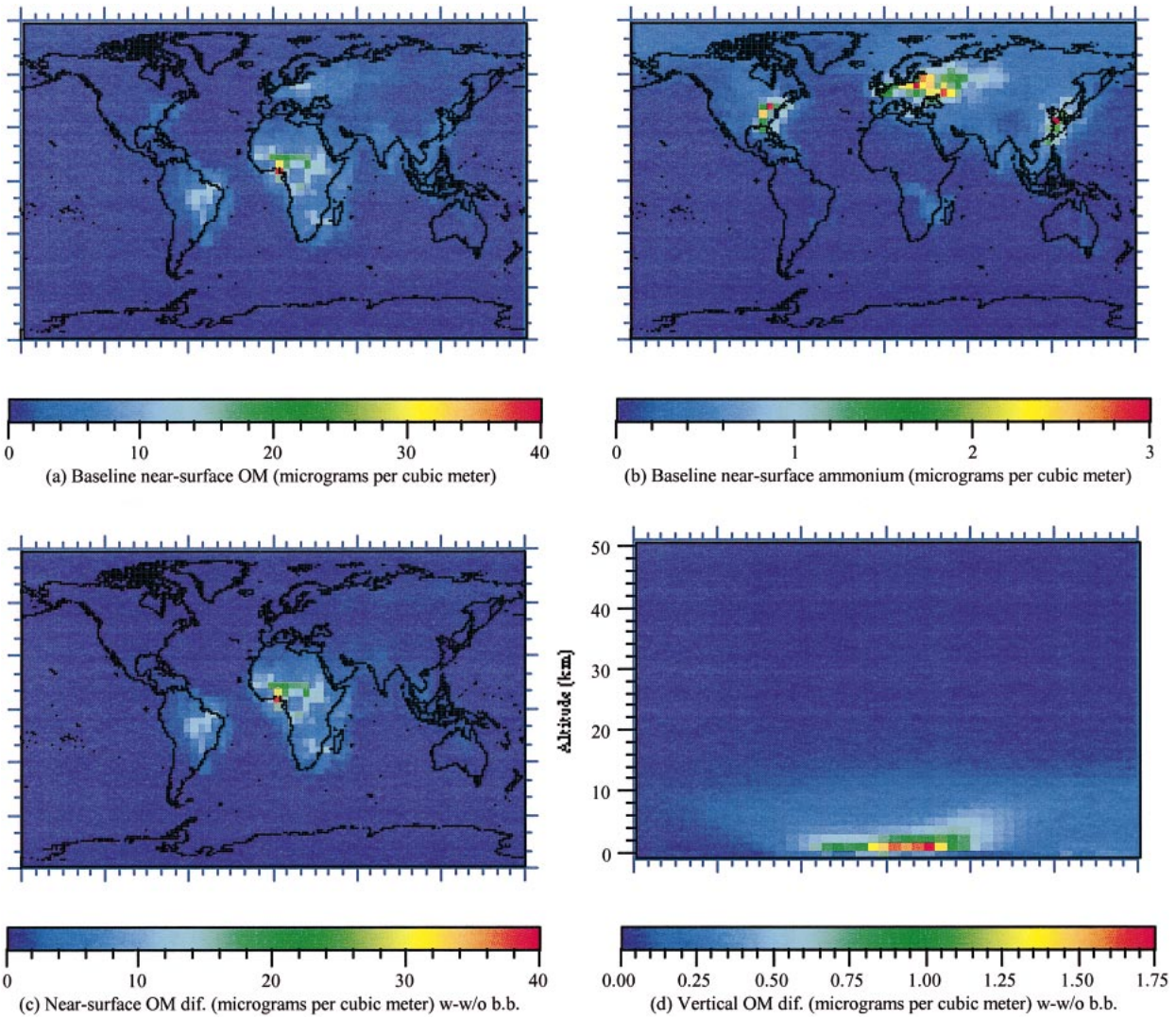

FIG. 4. Ten-year-averaged modeled (a) near-surface biomass-burning plus fossil-fuel OM (μg m^{-3}) from the baseline simulation, (b) near-surface NH_4^+ (μg m^{-3}) from all sources from the baseline simulation, (c) difference in near-surface OM (μg m^{-3}) when biomass-burning emissions were versus were not included in the calculation, and (d) difference in zonally averaged OM (μg m^{-3}) when biomass-burning emissions were versus were not included in the calculation.

Ketefian and M. Z. Jacobson 2004, unpublished manuscript), Sea surface temperatures were also affected by radiative and sensible heat, and latent heat fluxes.

4. Analysis of 10-yr climate-response simulations

A pair of 10-yr global climate-response simulations was run: one with gas and aerosol emissions from all anthropogenic and natural sources (baseline case) and one with all emissions except biomass-burning gas and particle emissions (sensitivity case).

Figures 4a and 4b show 10-yr averaged-modeled near-surface OM and NH_4^+ from the baseline case. Figures 4c and 4d show the 10-yr-average difference in near-surface and elevated OM between the baseline case and the no-biomass-burning case. Thus, Fig. 4c represents the contribution of biomass burning to OM. Difference plots for BC are similar to those for OM, but about a factor of 8 lower. Biomass-burning OM, was most prevalent in the Tropics of South America and Africa. Figure 4d suggests that burning produced tropospheric OM layers, which penetrated closer to the Arctic than Antarctic. Ammonium was high where S(VI) [$=H_2SO_4(aq) + HSO_4^- + SO_4^{2-}$] was high because ammonia gas dissolves readily in sulfuric-acid-containing particles. The highest ammonium concentrations were in Europe, which had high S(VI) concentrations.

Jacobson (2002a) compared modeled BC, S(VI), cloud water, precipitation, and cloud fraction with data. Figures 5a,b here show scatterplots of modeled versus measured near-surface OC and NH_4^+. Predictions, par-

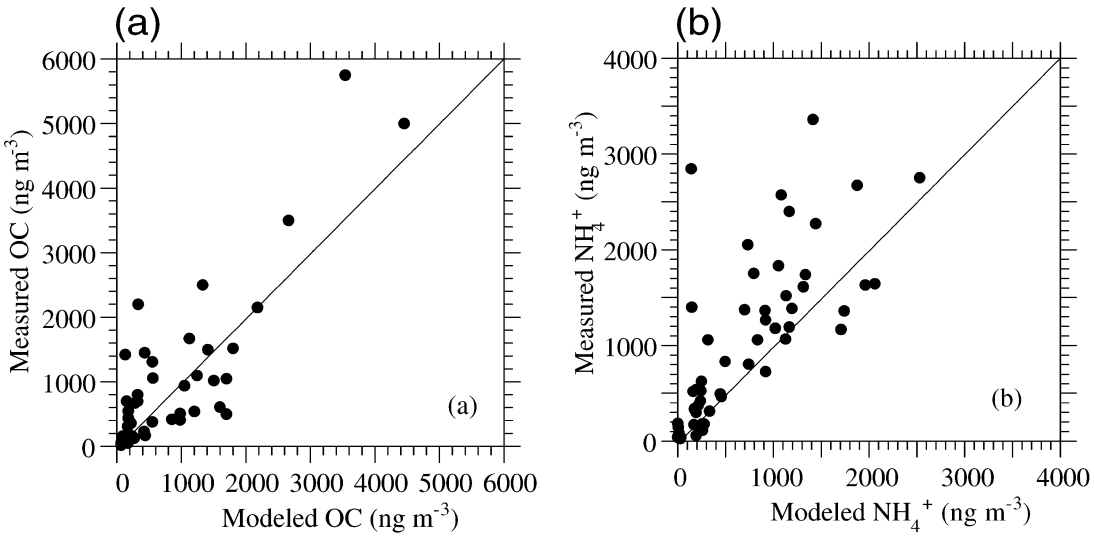

FIG. 5. Scatterplot of modeled versus measured near-surface (a) particulate organic carbon and (b) particulate ammonium concentrations at specific locations. Measured values were from Ketsidiris et al. (1976), Hoffman and Duce (1977), Chesselet et al. (1981), Andreae (1983), Dzubay et al. (1984), Andreae et al. (1984), Ohta and Okita (1984), Cachier et al. (1986, 1989, 1994), Wolff et al. (1986), Clarke (1989), Mukai et al. (1990), Keeler et al. (1990), Novakov and Penner (1993), Gaffney et al. (1984), McNaughton and Vet (1996), Hjellbrekke and Hanssen (1998), Heidam et al. (1999), Zappoli et al. (1999), B. M. Kim et al. (2000), Y. P. Kim et al. (2000), Puxbaum et al. (2000), Kerminen et al. (2000), Johansen et al. (2000), Quinn et al. (2001), Beine et al. (2001), Temesi et al. (2001), Hillamo et al. (2001), Krivacsy et al. (2001), and Chowdhury et al. (2001).

ticular of NH_4^+, were biased somewhat low in comparison with measurements. In the case of OC, the low bias may be due to low modeled secondary organic aerosol formation. Low NH_4^+ may be due to either high model calculations of other cations or low concentrations of anions in aerosol particles. NH_4^+ is not emitted substantially during biomass burning, so it is unlikely that errors in such emissions were important. It is possible that errors in its emission from other sources were important. Low biases may also be due to high boundary layer heights, meteorological factors, and model resolution.

Figures 6a and 6b show differences in near-surface Na+K+Mg+Ca (carried together as mole-equivalent Na) and S(VI), respectively, between the two simulations. These species all had biomass-burning and other emission sources. The increase in Na+K+Mg+Ca (Fig. 6a) in biomass-burning regions was due mostly to increases in K, the species with the greatest emission factor among the four (Ferek et al. 1998). Increases in particulate S(VI) (Fig. 6b) were due to 1) dissolution of biomass-emitted SO_2(g) in clouds and aerosols followed by aqueous oxidation, 2) oxidation of SO_2(g) emitted during biomass burning to H_2SO_4(g) followed by H_2SO_4(g) condensation, 3) direct emission of biomass-particulate S(VI), and 4) enhanced condensation of nonbiomass H_2SO_4(g) due to an increase in particle surface area from biomass burning. The mass emission rate of gas-phase SO_2(g) from biomass burning was about 3 times that of particulate S(VI) (Ferek et al. 1998).

Concentrations of S(VI), Na, K, Mg, and Ca were also slightly affected by feedbacks of biomass-burning aerosols to emission rates of sea spray, which contain these components. Specifically, Fig. 6c shows that biomass burning caused a 10-yr average change in air pressure and wind speed/direction globally, and sea-spray emission rates are driven almost entirely by wind speed. Soil dust and road dust emission rates are also driven by wind speed, so concentrations of these aerosol types were also affected by biomass-burning emissions.

The feedback of biomass burning to pressure and winds globally (feedback to large-scale meteorology) is due to several factors. First, biomass-burning aerosols and gases change the local vertical temperature profile and cloud amount, which change the vertical transfer of horizontal momentum (as well as energy and moisture), changing local wind speed and direction, thereby changing local pressure. Since mass must be conserved globally, local changes in pressure must be compensated for by pressure changes farther away (total surface air pressure in the model is conserved to machine precision). Changes in pressure farther away affect wind speeds and cloud formation, which affects radiative fields, etc., farther away. Second, nonnegligible quantities of biomass-burning particles and larger quantities of gases travel long distances, particularly aloft. These gases and particles affect clouds and radiative fields, which feed back directly to pressures and winds far away. Figure 6c suggests that biomass-burning-enhanced anticyclones in the subtropics of the Southern Hemisphere and reduced pressure near the poles.

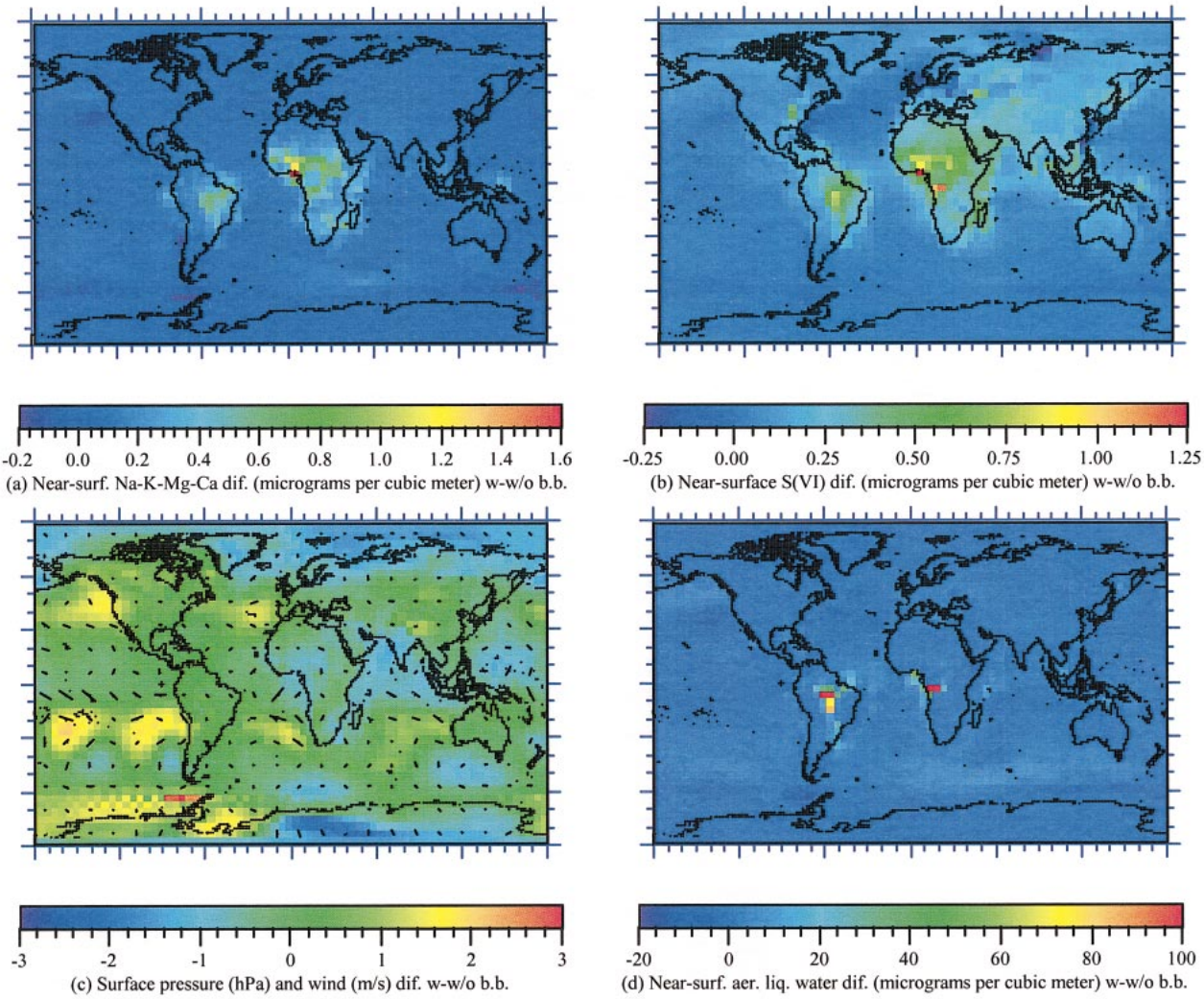

FIG. 6. Ten-year-averaged difference (when biomass-burning emissions were versus were not included) in (a) near-surface $Na^+ + K^+ + Mg^{2+} + Ca^{2+}$ ($\mu g\ m^{-3}$), (b) near-surface S(VI) ($\mu g\ m^{-3}$), (c) near-surface winds ($m\ s^{-1}$) and air pressure (hPa), (d) near-surface aerosol liquid water content ($\mu g\ m^{-3}$), (e) aerosol optical depth, (f) near-surface temperature (K), and (g) near-surface ozone (ppbv).

Figure 6d shows the difference in aerosol liquid water content (ALWC) due to biomass burning. The largest increase occurred in the Tropics, where the relative humidity (RH) was highest in the yearly average, but not exactly where the largest change in aerosol ion concentration occurred. Since ALWC is superlinearly dependent on RH for a given ion molality, a change in molality in a location of high RH can increase ALWC more than a larger change in molality in a location of low RH.

Figure 6e shows the difference in 10-yr-averaged aerosol optical depth (AOD). Maximum differences occurred roughly where ALWC changed the most. Modeled AODs included values within cloud and precipitation regions and outside of clouds when the relative humidity was near 100%. Since AODs increase rapidly near 100% relative humidity and drop tremendously where precipitation is occurring, modeled AODs may be higher or lower than measured or satellite-derived AODs, which filter cloud cover and relative humidities near 100%. Nevertheless, some comparisons of baseline-predicted AODs are given here. The average modeled baseline AOD over the global oceans was 0.115, slightly lower than the measured value of 0.12 (Husar et al. 1997). Modeled AODs over biomass-burning regions of Brazil and Africa during burning seasons ranged from 0.7 to 2.3 and 0.4 to 1.5, respectively, which compare with measured values of 0.9 to 2.1 over Brazil (Eck et al. 1998) and 0.7 to 1.7 over Zambia, (Eck et al. 2001), respectively. The modeled yearly averaged optical depth over Mongu, Zambia, was 0.19, which compares with a value of 0.24 from Eck et al.

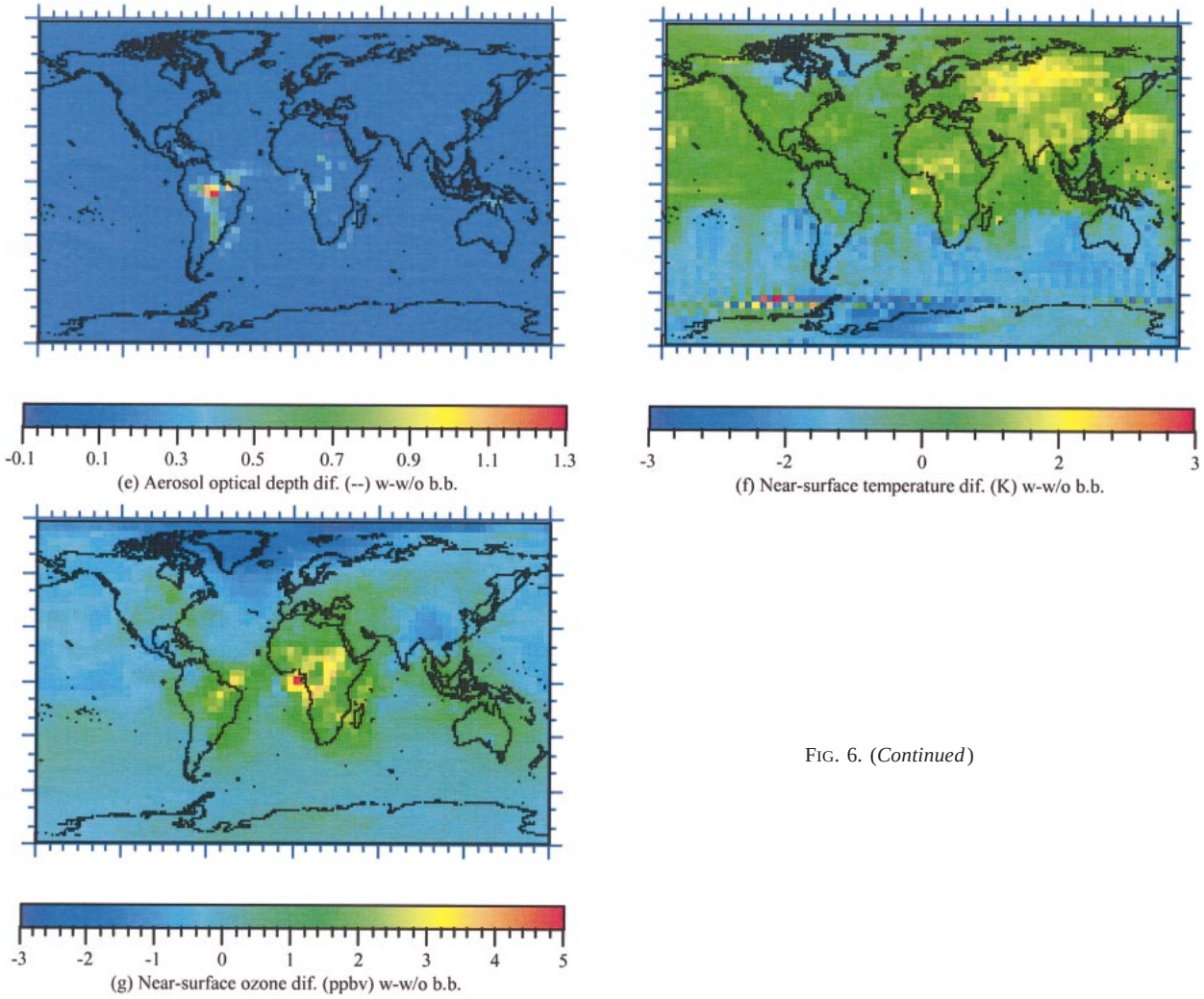

FIG. 6. (*Continued*)

(2003, Fig. 2). Modeled AODs over most other African regions south of the equator were lower than those derived in Torres et al. (2002), possibly due a dearth of modeled emissions in this region. Optical depths to the northwest of the Amazon River mouth were higher than those derived in Torres et al. (2002), possibly because modeled AODs were calculated at all relative humidities and in the presence of clouds, whereas the satellite product filters out relative humidities near 100% and clouds.

Table 1 shows that biomass burning decreased the

TABLE 1. Ten-year-averaged, globally averaged differences in several parameters resulting from the simulations when biomass-burning emissions were vs were not included.

Parameter	Difference	Parameter	Difference
Near-surface temperature	−0.14 K	Near-surface aerosol LWC	+1.5 μg m^{-3}
Near-surface RH	+0.00032 (of 1)	Near-surface BC	+0.12 μg m^{-3}
Surface albedo	+0.0009 (of 1)	Near-surface OM	+0.94 μg m^{-3}
Cloud optical depth	+0.28 (—)	Near-surface S(VI)	+0.11 μg m^{-3}
Cloud liquid water	−0.0006 kg m^{-2}	Near-surface NO_3^-	+0.042 μg m^{-3}
Cloud ice	−0.00008 kg m^{-2}	Near-surface Cl^-	+0.040 μg m^{-3}
Precipitation	−0.83 mm day^{-1}	Near-surface NH_4^+	+0.004 μg m^{-3}
Tropopause total Solar+IR forcing	−0.84 W m^{-2}	Near-surface $Na^+ + K^+ + Mg^{2+} + Ca^{2+}$	+0.063 μg m^{-3}
Aerosol optical depth	+0.043 (—)	Near-surface SO_2	+0.012 ppbv
Near surface aerosol Single scattering albedo	−0.026 (—)	Near-surface 0_3	+0.8 ppbv

globally and 10-yr-averaged aerosol single-scattering albedo (ASSA) by 0.026. Typical decreases near biomass-burning regions were 0.1. Baseline-modeled ASSAs ranged from 0.76 to 0.93 over Brazil and 0.79 to 0.91 over Africa, respectively, which compare with retrieved values of 0.79–0.95 (Dubovik et al. 1998) and 0.82–0.94 (Eck et al. 1998) over biomass-burning regions of Brazil, and of 0.82–0.85 over biomass-burning regions of Zambia (Eck et al. 2001).

Figure 6f shows the 10-yr-averaged modeled effect of biomass burning on near-surface temperatures. The major regions of cooling were throughout the Southern Hemisphere oceans from 15° to 80°S. The figure also shows some cooling over Brazil but some warming over Africa and Eastern Europe and regions of Asia. The temperature-change patterns due to biomass burning cannot be compared directly with observed temperature-change patterns because the latter are affected by all pollutants, which cause net warming, whereas the former are affected by a subset of pollutants, which cause short-term cooling. The warming in some biomass-burning regions and cooling in others is consistent with the fact that biomass burning may increase or decrease local temperatures (Tarasova et al. 1999). It also results because the plot shows a 10-yr average, whereas biomass burning occurs primarily in the dry season.

Some of the greatest temperature changes in the global and 10-yr average were over regions of snow and/or sea ice cover (e.g., northern Russia, northern Canada, and over the Antarctic continent and its sea ice). Changes in clouds and winds over these regions due to biomass burning (e.g., Fig. 6c) triggered changes in snow and sea ice cover, which changed albedo, which changed absorbed solar radiation, which changed ground temperature, which changed sensible and latent heat fluxes to the air, which changed air temperature.

Figure 6g shows the modeled change in near-surface ozone. Biomass burning increased ozone in biomass-burning regions. Ozone at high northern latitudes decreased somewhat most likely due to feedbacks to meteorology (Fig. 6c). The average increase over biomass-burning regions and the tropical southeastern Atlantic was about 5 ppbv, representing about a 25% increase over modeled background levels there. Mauzerall et al. (1998) found that biomass burning may have accounted for a 30% enhancement of ozone over the tropical South Atlantic during the dry season. In the global average, modeled ozone here increased by about 0.8 ppbv.

Figure 7a shows the difference in the globally and 10-yr-averaged layer and cumulative temperature due to biomass burning. The average or ''effective'' temperature of layer k from one simulation was calculated with

$$T_k = \frac{\sum_{i,j,t} V_{i,j,k,t}\rho_{a,i,j,k,t}c_{p,a}T_{i,j,k,t}}{\sum_{i,j,t} V_{i,j,k,t}\rho_{a,i,j,k,t}c_{p,a}}, \quad (16)$$

where the sums are over all grid cells i and j in the layer and over all time steps t during the averaging period, $V_{i,j,k,t}$ is the volume of a grid cell at a given time step and location, $\rho_{a,i,j,k,t}$ is the density of moist air (dry air plus water vapor) in a cell at a given time step, $c_{p,a}$ is the specific heat of moist air at constant pressure, and $T_{i,j,k,t}$ is the temperature in a cell. The difference in layer effective temperature from two simulations is the difference in Eq. (16) between two simulations. Equation (16) is used since temperature is a relative, not an absolute parameter, so the straight averaging of temperature from two different times or locations does not give the real average temperature because air density differs in each case. In Eq. (16), temperature is converted to energy, an absolute parameter. It can be refined further by considering the storage of energy in liquid water and ice, but that was not done here. The cumulative effective temperature from one simulation is the integrated effective temperature from the surface ($m = 1$) to the layer of interest (k):

$$T_{c,k} = \sum_{m=1}^{k} T_m. \quad (17)$$

The cumulative effective temperature at the stratopause is the integration of effective temperature from the surface to the stratopause. Layer temperatures in the stratosphere have little effect on cumulative temperature because air density is so low in the stratosphere that a large temperature change contributes little to total energy in the stratosphere [the numerator in Eq. (16)].

Figure 7a shows that biomass burning cooled the surface and upper stratosphere but warmed the upper troposphere/lower stratosphere, causing a slight cumulative atmospheric warming. The warming aloft occurred primarily in the Tropics, where most biomass burning occurred. It may have been due in large part to vertical transport of energy (e.g., due to changes in the Hadley cell circulation) or to a change in heating rate there. Figure 7e shows that, at the altitude of warming, the solar heating rate increased, but the thermal IR heating rate decreased. At that altitude, small changes in heating can trigger large changes in temperature due to the low air density. Changes in heating result from gradients in irradiance (Fig. 7f). The figure shows that the solar irradiance decreased at altitudes below 100 hPa.

Enhanced cloud scattering in the global average (Fig. 7b) was due to a decrease in the mean cloud-drop radius caused by the first indirect effect. At the same time, surface cooling (Fig. 7a) increased the stability of the lower and middle troposphere, decreasing cumulus convection, cloud liquid and ice (Fig. 7c), precipitation (Table 1), and vertical moisture fluxes from the ocean. The decrease in moisture flux reduced water vapor in the lower troposphere, but the suppression of convection reduced condensation and cloud liquid aloft, increasing water vapor aloft (Fig. 7d). The increase in scattering optical depth (Fig. 7b) with a decrease in cloud liquid in the global average (Table 1 and Fig. 7c) suggests that

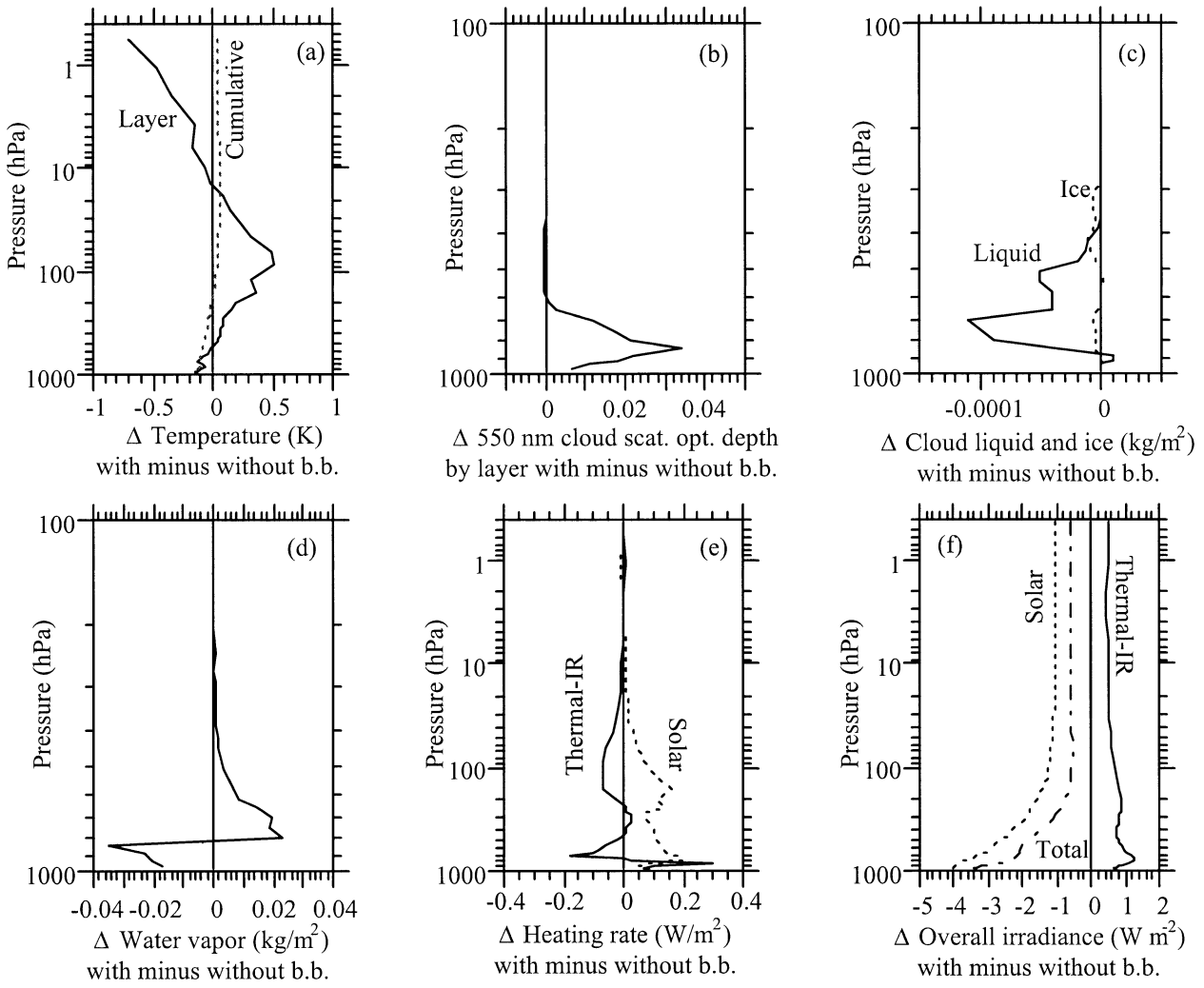

FIG. 7. (a) Ten-year-averaged difference in globally averaged layer and cumulative effective temperatures when all aerosols and gases were present vs when biomass-burning emissions were removed. Layer and cumulative effective temperatures were defined in Eqs. (16) and (17), respectively, and (a) shows differences in such temperatures from two simulations. The bottommost ''layer'' temperature change shown is the ground-temperature change, which is not included in the cumulative temperature change curves. The remaining curves are global differences from the simulations with minus without biomass burning for (b) cloud scattering optical depth, (c) cloud liquid and ice, (d) water vapor, (e) solar and thermal IR heating rates, and (f) net downward minus upward solar, thermal IR, and total irradiance (accounting for all feedbacks).

the decrease in drop radius had a greater effect on optical depth than did the decrease in cloud liquid.

The baseline average top-of-the-atmosphere solar and thermal IR radiative fluxes were 240 and -233 W m^{-2}, respectively, which compares with measurements of 238 and -235 W m^{-2}, respectively (Kiehl et al. 1998). The baseline surface solar and thermal-IR radiative fluxes were 165 and -67 W m^{-2}, respectively, which compares with measurements of 168 and -66 W m^{-2}, respectively (Kiehl and Trenberth 1997). Figure 7f shows that the 10-yr-averaged tropopause (at about 250 hPa) total forcing (direct forcing plus feedbacks) due to biomass-burning gases and aerosols was -0.84 W m^{-2} (in the last 5 yr of simulation, it was -0.6 to -1.2 W m^{-2}). Houghton et al. (2001) estimates a direct forcing from biomass-burning aerosols of -0.3 W m^{-2} and an indirect forcing from all aerosols of 0 to -2 W m^{-2}. Assuming crudely that biomass-burning indirect forcing represents 23%–29% of total indirect forcing (assuming a similar ratio of biomass burning to total anthropogenic particle emissions as the ratio of biomass burning to total anthropogenic CO_2 emissions), the short-term model forcing estimate is within the range of a rough value extracted from IPCC.

Figure 8 (solid line) shows the globally averaged time-dependent response of eliminating biomass-burning aerosols and short-lived gases from the 10-yr base simulation described in section 4. Eliminating biomass burning caused fluctuations in global temperatures in years 1–5 but less so in years 8–10, where the differ-

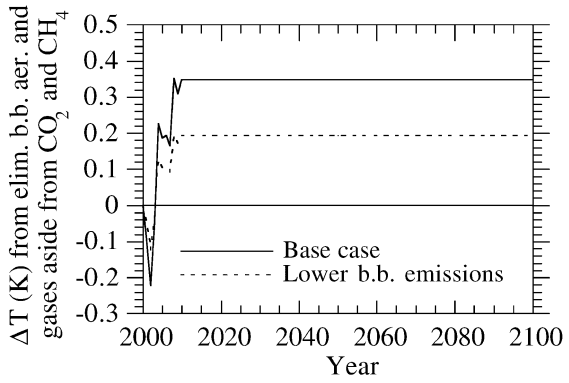

FIG. 8. Solid line: Calculated temperature change, over 10 yr, due to eliminating biomass-burning particles and gases but ignoring the radiative effects of CH_4 and CO_2. The change in temperature from years 10 to 100 was held to that in year 10. Dashed line: Base case scaled by 0.555 to approximate the effect of the lower biomass-burning emission estimate (section 4).

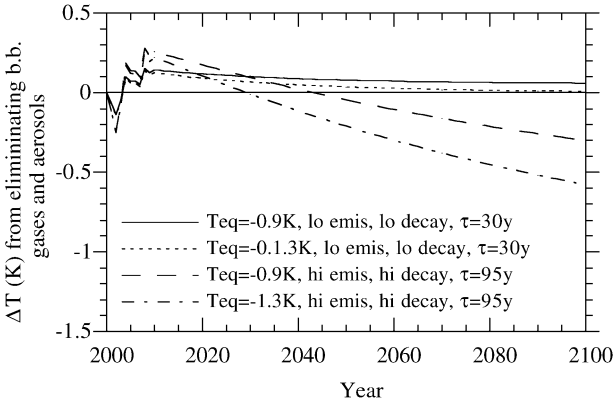

FIG. 9. Estimated temperature change over 100 yr due to eliminating all biomass-burning gas and particle emissions, determined by summing the curves in Figs. 3a, 3b, and 8. The flat line represents zero change in temperature.

ences were +0.35, +0.31, and +0.35 K, respectively. The 10-yr average change due to eliminating burning was +0.14 K (Table 1). The changes in temperature from years 11 to 100 were held to the highest value from years 1 to 10. If the average value over 10 yr was used (+0.14 K), the conclusion would be stronger than that obtained. The dashed line in Fig. 8 is the base-case response, scaled by 55.5% (the ratio of the lower to upper bound of CO_2 emission, 1500:2700 Tg CO_2–C yr^{-1}) to account for the lower bound in the estimate of the biomass-burning emission rate. Although an emission change will result in some different feedbacks, rerunning the base case at a lower emission was not done due to computational constraints.

Although biomass and fossil-fuel burning emit roughly equivalent levels of BC globally, the modeled short-term climate response of biomass burning (cooling of −0.35 K in year 10) was opposite from that of fossil fuel (ff) BC+OM emissions calculated in Jacobson (2002a) (warming of +0.35 K in year 5, the last year of the simulation). Although biomass-burning BC suppresses cooling in biomass particles, such particles contain much more OM, K^+, Na^+, Ca^{2+}, Mg^{2+}, NH_4^+, Cl^-, SO_4^{2-}, and NO_3^- than do fossil-fuel soot particles. In addition, the OM:BC in biomass-burning particles (8:1) is much larger than that in fossil-fuel soot particles (0.5:1 to 3:1). Whereas many biomass-burning components, including organics, are hygroscopic, the OM in diesel soot, for example, is primarily lubricating oil (e.g., Kittelson 1998). As such, newly emitted soot particles do not absorb much water (Weingartner et al. 1997) and are poor cloud condensation nuclei (Ishizaka and Adhikari 2003). Biomass-burning particles, while not so hygroscopic as pure sulfate particles, are more hygroscopic and better cloud condensation nuclei than are fossil-fuel soot particles, allowing biomass particles to scatter more and form clouds better than soot particles do. Finally, since the thermally driven circulation in the Tropics affects global circulation, perturbations in the Tropics may feed back to the larger scale more than perturbations elsewhere.

5. Combining 10- and 100-yr results

Figure 9 shows the overall climate response of biomass burning over 100 yr, determined by summing the climate responses of CO_2, CH_4, and aerosols/short-lived gases from Figs. 3a, 3b, and 8, respectively. Curves with the same emission rates are summed consistently. The result accounts for a range of biomass-burning CO_2 emission of 1500–2700 Tg CO_2–C yr^{-1}, a corresponding range biomass-burning aerosol emission, biological decay emission 1–3 times those of direct forest-burning emission, overall lifetime of CO_2 30–95 yr, and an equilibrium climate response of removing anthropogenic CO_2 of −0.9 to −0.13 K. The envelope of climate responses suggests a global cooling a few decades after biomass burning is first controlled in almost all cases.

A factor not accounted for is the effect of the deep ocean on air temperatures. In Jacobson (2002a), it was suggested that energy transport to the deep ocean affects the climate response of individual components proportionally to the magnitude of the initial response. If two components cause warming, the deep ocean will dampen the warming of stronger warming more due to enhanced stratification. If one component causes cooling and the other warming, the deep ocean will reduce the magnitude of cooling and warming but not change the sign of either.

To test this theory, vertical one-dimensional advection–diffusion simulations of mixing to the deep ocean of a temperature perturbation to the mixed layer were run for 100 yr. A vertical velocity of 4 m yr^{-1} (Hoffert et al. 1980) and three diffusion coefficients (0, 1×10^{-5}, and 1×10^{-4} m^2 s^{-1}) were used. The 1×10^{-4} m^2 s^{-1} value is close to the canonical globally averaged deep-ocean value, but the global value is really a combination

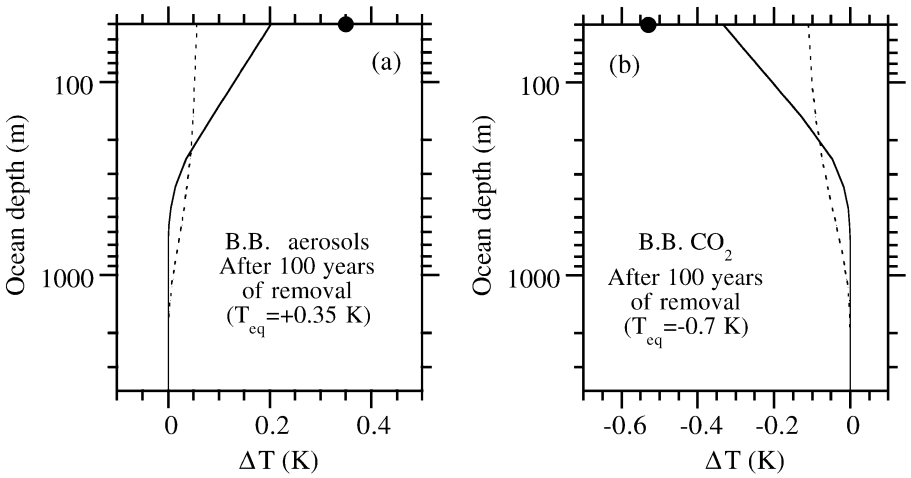

FIG. 10. Vertical profile 100 yr after imposing a time-dependent temperature perturbation to the mixed layer of the ocean (top 100 m) of the form $\Delta T_m(t + h) = T_{eq}[\exp(-t/\tau) - \exp(-(t + h)/\tau]$, where t is the time from start (yr), h is the time step (yr), T_{eq} (set to $+0.35$ K for biomass-burning aerosols and -0.7 K for CO_2) is the equilibrium temperature perturbation to the ocean, and τ (set to 4 yr for biomass-burning aerosols and 70 yr for CO_2) is the relaxation e-folding time required to reach equilibrium. The three results shown for each case are (i) no vertical diffusion or vertical velocity (solid dot), (ii) $K = 1 \times 10^{-5}$ m^2 s^{-1} and $w = 4$ m yr^{-1} (solid line), and (iii) $K = 1 \times 10^{-4}$ m^2 s^{-1} (2000 m^2 yr^{-1}) and $w = 4$ m yr^{-1} (dashed line). Profiles with assumptions (ii) and (iii) were found by solving the one-dimensional advection diffusion equation after discretizing the ocean into forty 100-m deep ocean layers and one 100-m ocean mixed layer and using a time step of $h = 5$ days (0.0137 yr).

of smaller values (e.g., 1×10^{-5} m^2 s^{-1}) over possibly 99% of the ocean and larger values (e.g., 1×10^{-2} m^2 s^{-1}) over the remaining 1% of the ocean (Kantha and Clayson 2000, p. 679; Kunze and Sanford 1996). The larger values occur primarily near sloping topography and comprise most of the mixing.

Two sets of simulations are shown, one for biomass-burning aerosols with an equilibrium warming upon removal of $+0.35$ K (from the high-emission-rate case in Fig. 8) and an e-folding time of 4 yr to obtain this temperature and one for biomass-burning CO_2 with an equilibrium cooling upon removal of -0.7 K and an e-folding time of 70 yr to obtain this response (which gives a cooling after 100 yr of -0.53 K, a middle value in Fig. 3a). Figure 10 shows the vertical profile of each perturbation after 100 yr for each of the three diffusion coefficients. In all cases, the damping of mixed layer temperature was proportional to the magnitude of the initial perturbation. The magnitude of cooling due to removing CO_2 was larger than the magnitude of the warming due to removing aerosols. This result held for both low and high diffusion coefficients. In sum, inclusion of the deep ocean should dampen all atmospheric temperature perturbations proportionally to the magnitude of the perturbation. Thus, neglecting the deep ocean should have marginal effect on the timing between the switchover between warming and cooling and little effect on the main conclusion of this study.

6. Conclusions

The Kyoto Protocol of 1997 did not consider controlling biomass burning as a strategy for slowing global warming. This study suggests that such a strategy may be beneficial. It finds that, whereas aerosol particles emitted during burning may cause a short-term cooling of global climate, longer-lived greenhouse gases may cause warming (or cancel the cooling) after several decades. As such, reducing biomass burning may cause short-term warming but long-term cooling or no change in temperature. Although the eventual cooling may not appear for many years, its magnitude may be as large as 0.6 K after 100 yr. Much of this reduction would be due to eliminating future increases in CO_2 from biomass burning. By far the greatest long-term benefit in reducing biomass burning would result from the reduction in permanent deforestation. For example, of all CO_2 reduced after 100 yr due to stopping biomass burning, 94%–97% was calculated to be due to eliminating permanent forest burning/decay, 2%–4% was due to eliminating temporary forest burning/decay, 0.8%–2% was due to eliminating savannah burning, and 0.1%–0.3% was due to eliminating agricultural burning. Results, though, are subject to model and emission uncertainties and require further verification.

Although savannah and agricultural burning contribute less to CO_2 than does permanent forest burning in the long term, both still result in some CO_2 accumu-

lation. In fact, for any century-scale time lag between biomass burning and full regrowth, burning results in an accumulation of CO_2. Fertilization modifies this accumulation but does not eliminate it. Since grassland and cropland burned yearly as opposed to every several years increase CO_2, biofuels, considered ''renewable,'' are only partially renewable, and even temporary biomass burning always results in elevated CO_2 until it is stopped.

Although controlling biomass burning may not be so efficient at slowing global warming in terms of the speed and magnitude of its effect, as controlling fossil-fuel black carbon, it is necessary to address multiple causes of warming simultaneously. Because aerosol particles may be the most damaging and costly components of air pollution (e.g., Spadaro and Rabl 2001), reducing both biomass burning and ff BC+OM may reduce health problems and mortality. It is beyond the scope of this paper to examine specific control strategies, but the historical record suggests that emission problems can be reduced through national and international regulation and market incentives.

Acknowledgments. This work was supported by the Environmental Protection Agency, the NASA New Investigator Program in Earth Sciences, the National Science Foundation, and the David and Lucile Packard Foundation and the Hewlett-Packard Company.

REFERENCES

Andreae, M. O., 1983: Soot carbon and excess fine potassium: Long-range transport of combustion-derived aerosols. *Science,* **220,** 1148–1151.

——, and P. Merlet, 2001: Emission of trace gases and aerosols from biomass burning. *Global Biogeochem. Cycles,* **15,** 955–966.

——, T. W. Andreae, R. J. Ferek, and H. Raemdonck, 1984: Long range transport of soot carbon in the marine atmosphere. *Sci. Total Environ.,* **36,** 73–80.

Beine, H., I. Allegrini, R. Sparapani, A. Ianniello, and F. Valentini, 2001: Three years of springtime trace gas and particle measurements at Ny-Alesund, Svalbard. *Atmos. Environ.,* **35,** 3645–3658.

Bolin, B., and R. Sukumar, 2000: Global perspective. *Land Use, Land-Use Change, and Forestry,* R. T. Watson et al., Eds., Cambridge University Press, 24–51.

Bond, T. C., D. G. Streets, K. F. Yarber, S. M. Nelson, J.-H. Woo, and Z. Kilmont, 2004: A technology-based global inventory of black and organic carbon emissions from combustion. *J. Geophys. Res.,* in press.

Cachier, H., P. Buat-Ménard, M. Fontugne, and R. Chesselet, 1986: Long-range transport of continentally-derived particulate carbon in the marine atmosphere: Evidence from stable carbon isotope studies. *Tellus,* **38B,** 161–177.

——, M.-P. Brémond, and P. Buat-Ménard, 1989: Determination of atmospheric soot carbon with a simple thermal method. *Tellus,* **41B,** 379–390.

——, C. Liousse, A. Cachier, B. Ardouin, G. Polian, V. Kazan, and A. D. Hansen, 1994: A. Black carbon aerosols at the remote site of Amsterdam Island. *Proc. Fifth Int. Conf. on Carbonaceous Aerosols,* Berkeley, CA, U.S. Dept. of Energy.

Carvalho, J. A., Jr., N. Higuchi, T. M. Araujo, and J. C. Santos, 1998: Combustion completeness in a rainforest clearing experiment in Manaus, Brazil. *J. Geophys. Res.,* **103,** 13 195–13 199.

——, F. S. Costa, C. A. Gurgel Veras, D. Sandberg, E. C. Alvarado, R. Gielow, A. M. Serra Jr., and J. C. Saros, 2001: Biomass fire consumption and carbon release rates of rainforest clearing experiments conducted in northern Mato Grosso, Brazil. *J. Geophys. Res.,* **106,** 17 877–17 887.

Chesselet, R., M. Fontugne, P. Buat-Ménard, U. Ezat, and C. E. Lambert, 1981: The origin of particulate organic carbon in the marine atmosphere as indicated by its stable carbon isotopic composition. *Geophys. Res. Lett.,* **8,** 345–348.

Chowdhury, Z., L. S. Hughes, L. G. Salmon, and G. R. Cass, 2001: Atmospheric particle size and composition measurements to support light extinction calculations over the Indian Ocean. *J. Geophys. Res.,* **106,** 28 597–28 605.

Christopher, S. A., J. Chou, J. Zhang, X. Li, T. A. Berendes, and R. M. Welch, 2000a: Shortwave direct radiative forcing of biomass burning aerosols estimated using VIRS and CERES data. *Geophys. Res. Lett.,* **27,** 2197–2200.

——, X. Li, R. M. Welch, J. S. Reid, P. V. Hobbs, T. F. Eck, and B. Holben, 2000b: Estimation of surface and top-of-atmosphere shortwave irradiance in biomass-burning regions during SCAR-B. *J. Appl. Meteor.,* **39,** 1742–1753.

Clarke, A. D., 1989: Aerosol light absorption by soot in remote environments. *Aerosol Sci. Technol.,* **10,** 161–171.

Cooke, W. F., and J. J. N. Wilson, 1996: A global black carbon aerosol model. *J. Geophys. Res.,* **101,** 19 395–19 409.

Crutzen, P. J., and M. O. Andreae, 1990: Biomass burning in the Tropics: Impact on atmospheric chemistry and biogeochemical cycles. *Science,* **21,** 1669–1677.

Ding, P., and D. A. Randall, 1998: A cumulus parameterization with multiple cloud-base levels. *J. Geophys. Res.,* **103,** 11 341–11 353.

Dubovik, O., B. N. Holben, Y. J. Kaufman, M. Yamasoe, A. Smirnov, D. Tanre, and I. Slutsker, 1998: Single-scattering albedo of smoke retrieved from the sky radiance and solar transmittance measured from ground. *J. Geophys. Res.,* **103,** 31 903–31 923.

——, ——, T. F. Eck, A. Smirnov, Y. J. Kaufman, M. D. King, D. Tanre, and I. Slutsker, 2002: Variability of absorption and optical properties of key aerosol types observed in worldwide locations. *J. Atmos. Sci.,* **59,** 590–608.

Dzubay, T. G., R. K. Stevens, and P. L. Haagenson, 1984: Composition and origins of aerosol at a forested mountain in Soviet Georgia. *Environ. Sci. Technol.,* **18,** 873–883.

Eck, T. F., B. N. Holben, I. Slutsker, and A. Setzer, 1998: Measurements of irradiance attenuation and estimation of aerosol single scattering albedo for biomass burning aerosols in Amazonia. *J. Geophys. Res.,* **103,** 31 865–31 878.

——, and Coauthors, 2001: Characterization of the optical properties of biomass burning aerosols in Zambia during the 1997 ZIBBEE field campaign. *J. Geophys. Res.,* **106,** 3425–3448.

——, and Coauthors, 2003: Variability of biomass burning aerosol optical characteristics in southern Africa during the SAFARI 2000 dry season campaign and a comparison of single scattering albedo estimates from radiometric measurements. *J. Geophys. Res.,* **108,** 8477, doi:10.1029/2002JD002321.

Ferek, R. J., J. S. Reid, P. V. Hobbs, D. R. Blake, and C. Liousse, 1998: Emission factors of hydrocarbons, halocarbons, trace gases and particles from biomass burning in Brazil. *J. Geophys. Res.,* **103,** 32 107–32 118.

Gaffney, J. S., R. L. Tanner, and M. Phillips, 1984: Separating carbonaceous aerosol source terms using thermal evolution, carbon isotropic measurements, and C/N/S determinations. *Sci. Total Environ.,* **36,** 53–60.

Grant, K. E., C. C. Chuang, A. S. Grossman, and J. E. Penner, 1999: Modeling the spectral optical properties of ammonium sulfate and biomass burning aerosols: Parameterization of relative humidity effects and model results. *Atmos. Environ.,* **33,** 2603–2620.

Hao, W. M., and M.-H. Liu, 1994: Spatial and temporal distribution of tropical biomass burning. *Global Biogeochem. Cycles,* **8,** 495–503.

Harmon, M. E., W. K. Ferrell, and J. F. Franklin, 1990: Effects on

carbon storage of conversion of old-growth forests to young forests. *Science,* **247,** 699–702.
Heidam, N. Z., P. Wahlin, and J. H. Christensen, 1999: Tropospheric gases and aerosols in northeast Greenland. *J. Atmos. Sci.,* **56,** 261–278.
Hillamo, R., V.-M. Kerminen, M. Aurela, T. Makela, W. Maenhaut, and C. Leck, 2001: Modal structure of chemical mass size distribution in the high Arctic aerosol. *J. Geophys. Res.,* **106,** 27 555–27 571.
Hjellbrekke, A.-G., and J. E. Hanssen, 1998: 1996 data report. 1. Annual summaries. EMEP/CCC Rep. 1/98, 85 pp. [Available from Norwegian Institute for Air Research, Lillestrom, Norway.]
Hobbs, P. V., J. S. Reid, R. A. Kotchenruther, R. J. Ferek, and R. Weiss, 1997: Direct radiative forcing by smoke from biomass burning. *Science,* **275,** 1776–1778.
Hoffert, M. I., A. J. Callegari, and C.-T. Hsieh, 1980: The role of deep sea heat storage in the secular response of climatic forcing. *J. Geophys. Res.,* **85,** 6667–6679.
Hoffman, E. J., and R. A. Duce, 1977: Organic carbon in marine atmospheric particulate matter: Concentration and particle size distribution. *Geophys. Res. Lett.,* **4,** 449–452.
Houghton, J. T., Y. Ding, D. J. Griggs, M. Noguer, P. J. Van der Linden, X. Dai, K. Maskell, and C. A. Johnson, Eds., 2001: *Climate Change 2001: The Scientific Basis.* Cambridge University Press, 881 pp.
Houghton, R. A., 1999: The annual net flux of carbon to the atmosphere from changes in land use 1850–1990. *Tellus,* **51B,** 298–313.
——, D. L. Skole, C. A. Nobre, J. L. Hackler, K. T. Lawrence, and W. H. Chomentowski, 2000: Annual fluxes of carbon from deforestation and regrowth in the Brazilian Amazon. *Nature,* **403,** 301–304.
Husar, R. B., J. M. Prospero, and L. L. Stowe, 1997: Characterization of tropospheric aerosols over the oceans with the NOAA Advanced Very High Resolution Radiometer optical thickness operational product. *J. Geophys. Res.,* **102,** 16 889–16 909.
Iacobellis, S. F., R. Frouin, and R. C. J. Somerville, 1999: Direct climate forcing by biomass-burning aerosols: Impact of correlations between controlling variables. *J. Geophys. Res.,* **104,** 12 031–12 045.
Ishizaka, Y., and M. Adhikari, 2003: Composition of cloud condensation nuclei. *J. Geophys. Res.,* **108,** 4138, doi:10.1029/2002JD002085.
Jacobson, M. Z., 1997: Development and application of a new air pollution modeling system—Part III. Aerosol-phase simulations. *Atmos. Environ.,* **31,** 587–608.
——, 2001a: GATOR-GCMM: A global-through urban-scale air pollution and weather forecast model. Part 1: Model design and treatment of subgrid soil, vegetation, roads, rooftops, water, sea ice, and snow. *J. Geophys. Res.,* **106,** 5385–5401.
——, 2001b: GATOR-GCMM: A study of daytime and nighttime ozone layers aloft, ozone in national parks, and weather during the SARMAP field campaign. *J. Geophys. Res.,* **106,** 5403–5420.
——, 2001c: Global direct radiative forcing due to multicomponent anthropogenic and natural aerosols. *J. Geophys. Res.,* **106,** 1551–1568.
——, 2001d: Strong radiative heating due to the mixing state of black carbon in atmospheric aerosols. *Nature,* **409,** 695–697.
——, 2002a: Control of fossil-fuel particulate black carbon and organic matter, possibly the most effective method of slowing global warming. *J. Geophys. Res.,* **107,** 4410, doi:10.1029/2001JD001376.
——, 2002b: Analysis of aerosol interactions with numerical techniques for solving coagulation, nucleation, condensation, dissolution, and reversible chemistry among multiple size distributions. *J. Geophys. Res.,* **107,** 4366, doi:10.1029/2001JD002044.
——, 2003: Development of mixed-phase clouds from multiple aerosol size distributions and the effect of the clouds on aerosol removal. *J. Geophys. Res.,* **108,** 4245, doi:10.1029/2002JD002691.
——, cited 2004: Updates to ''Control of fossil-fuel particulate black carbon and organic matter, possibly the most effective method of slowing global warming.'' [Available online at http://www.stanford.edu/group/efmh/fossil/fossil.html.]
Johansen, A. M., R. L. Siefert, and M. R. Hoffmann, 2000: Chemical composition of aerosols collected over the tropical North Atlantic Ocean. *J. Geophys. Res.,* **105,** 15 277–15 312.
Kantha, L. H., and C. A. Clayson, 2000: *Small Scale Processes in Geophysical Fluid Flows.* Academic Press, 888 pp.
Kauffman, J. B., D. L. Cummings, D. E. Ward, and R. Babbitt, 1995: Fire in the Brazilian Amazon: 1. Biomass, nutrient pools, and losses in slashed primary forests. *Oecologia,* **104,** 397–408.
Kaufman, Y. J., and R. S. Fraser, 1997: The effect of smoke particles on clouds and climate forcing. *Science,* **277,** 1636–1639.
Keeler, G. J., S. M. Japar, W. W. Brachaczek, R. A. Gorse, J. M. Norbeck, and W. R. Pierson, 1990: The sources of aerosol elemental carbon at Allegheny Mountain. *Atmos. Environ.,* **24A,** 2795–2805.
Kerminen, V.-M., K. Teinila, and R. Hillamo, 2000: Chemistry of sea-salt particles in the summer Antarctic atmosphere. *Atmos. Environ.,* **34,** 2817–2825.
Ketsidiris, G., J. Hahn, R. Jaenicke, and C. Junge, 1976: The organic constituents of atmospheric particulate matter. *Atmos. Environ.,* **10,** 603–610.
Kiehl, J. T., and K. E. Trenberth, 1997: Earth's annual global mean energy budget. *Bull. Amer. Meteor. Soc.,* **78,** 197–208.
——, J. J. Hack, G. B. Bonan, B. A. Boville, D. L. Williamson, and P. J. Rasch, 1998: The National Center for Atmospheric Research Community Climate Model: CCM3. *J. Climate,* **11,** 1131–1149.
Kim, B. M., S. Teffera, and M. D. Zeldin, 2000: Characterization of $PM_{2.5}$ and PM_{10} in the South Coast Air Basin of Southern California: Part 1—Spatial variations. *J. Air Waste Manage. Assoc.,* **50,** 2034–2044.
Kim, Y. P., K.-C. Moon, and J. H. Lee, 2000: Organic and elemental carbon in fine particles at Kosan, Korea. *Atmos. Environ.,* **34,** 3309–3317.
Kittelson, D. B., 1998: Engine and nanoparticles: A review. *J. Aerosol Sci.,* **6,** 443–451.
Kreidenweis, S. M., L. A. Remer, R. Bruintjes, and O. Dubovik, 2001: Smoke aerosol from biomass burning in Mexico: Hygroscopic smoke optical model. *J. Geophys. Res.,* **106,** 4831–4844.
Krivacsy, Z., and Coauthors, 2001: Role of organic and black carbon in the chemical composition of atmospheric aerosol at European background sites. *Atmos. Environ.,* **35,** 6231–6244.
Kunze, E., and T. B. Sanford, 1996: Abyssal mixing: Where it is not. *J. Phys. Oceanogr.,* **26,** 2286–2296.
Liousse, C., J. E. Penner, J. J. Walton, H. Eddleman, C. Chuang, and H. Cachier, 1996: Modeling biomass burning aerosols. *Biomass Burning and Global Change,* J. S. Levine, Ed., MIT Press, 492–508.
Mari, C., D. J. Jacob, and P. Bechtold, 2000: Transport and scavenging of soluble gases in a deep convective cloud. *J. Geophys. Res.,* **105,** 22 255–22 267.
Marland, G., T. A. Boden, and R. J. Andres, 2003: Global, regional, and national CO_2 emissions. *Trends: A Compendium of Data on Global Change,* Carbon Dioxide Information Analysis Center, Oak Ridge National Laboratory. [Available online at http://cdiac.esd.ornl/.gov/trends/emis/meth_reg.htm.]
Mauzerall, D. L., and Coauthors, 1998: Photochemistry in biomass burning plumes and implications for tropospheric ozone over the tropical South Atlantic. *J. Geophys. Res.,* **103,** 8401–8423.
McNaughton, D. J., and R. J. Vet, 1996: Eulerian model evaluation field study (EMEFS): A summary of surface network measurements and data quality. *Atmos. Environ.,* **30,** 227–238.
Mukai, H., Y. Ambe, K. Shibata, T. Muku, K. Takeshita, T. Fukuma, J. Takahashi, and S. Mizota, 1990: Long term variation of chemical composition of atmospheric aerosol on the Oki Islands in the Sea of Japan. *Atmos. Environ.,* **24A,** 1379–1390.
NCEP, 2002: 2.5 degree global final analyses. Data Support Section, National Center for Atmospheric Research.
Novakov, T., and J. E. Penner, 1993: Large contributions of organic

aerosols to cloud-condensation nuclei concentrations. *Nature,* **365,** 823–826.

Ohta, S., and T. Okita, 1984: Measurements of particulate carbon from the atmosphere. *Sci. Total Environ.,* **18,** 2439–2445.

Penner, J. E., R. E. Dickinson, and C. A. O'Neill, 1992: Effects of aerosol from biomass burning on the global radiation budget. *Science,* **256,** 1432–1434.

——, C. C. Chuang, and K. Grant, 1998: Climate forcing by carbonaceous and sulfate aerosols. *Climate Dyn.,* **14,** 839–851.

Poorter, H., 1993: Interspecific variation in the growth response of plants to an elevated ambient CO_2 concentration. *Vegetatio,* **104/105,** 77–97.

Puxbaum, H., J. Rendl, R. Allabashi, L. Otter, and M. C. Scholes, 2000: Mass balance of the atmospheric aerosol in a South African subtropical savanna (Nylsvley, May 1997). *J. Geophys. Res.,* **105,** 20 697–20 706.

Quinn, P. K., D. J. Coffman, T. S. Bates, T. L. Miller, J. E. Johnson, K. Voss, E. J. Welton, and C. Neusus, 2001: Dominant aerosol chemical components and their contribution to extinction during the Aerosols99 cruise across the Atlantic. *J. Geophys. Res.,* **106,** 20 783–20 809.

Reid, J. S., and P. V. Hobbs, 1998: Physical and optical properties of young smoke from individual biomass fires in Brazil. *J. Geophys. Res.,* **103,** 32 013–32 030.

Robock, A., 1988: Enhancement of surface cooling due to forest fire smoke. *Science,* **242,** 911–913.

Ross, J. L., P. V. Hobbs, and B. Holben, 1998: Radiative characteristics of regional hazes dominated by smoke from biomass burning in Brazil: Closure tests and direct radiative forcing. *J. Geophys. Res.,* **103,** 31 925–31 941.

Schlamadinger, B., and T. Karjalainen, 2000: Afforestation, reforestation, and deforestation (ARD) activities. *Land Use, Land-Use Change, and Forestry,* R. T. Watson et al., Eds., Cambridge University Press, 127–179.

Spadaro, J. V., and A. Rabl, 2001: Damage costs due to automotive air pollution and the influence of street canyons. *Atmos. Environ.,* **35,** 4763–4775.

Stern, D. I., and R. K. Kaufman, 1998: Annual estimates of global anthropogenic methane emissions: 1860–1994. *Trends Online: A Compendium of Data on Global Change,* Carbon Dioxide Information Analysis Center, Oak Ridge National Laboratory. [Available online at http://cdiac.esd.ornl.gov/trends/meth/ch4.htm.]

Stocks, B. J., and Coauthors, 1998: Climate change and forest fire potential in Russian and Canadian boreal forests. *Climatic Change,* **38,** 1–13.

Tarasova, T. A., C. A. Nobre, B. N. Holben, T. F. Eck, and A. Setzer, 1999: Assessment of smoke aerosol impact on surface solar irradiance measured in the Rondonia region of Brazil during Smoke, Clouds, and Radiation—Brazil. *J. Geophys. Res.,* **104,** 19 161–19 170.

Temesi, D., A. Molnar, E. Meszaros, T. Feczko, A. Gelencser, G. Kiss, and Z. Krivacsy, 2001: Size resolved chemical mass balance of aerosol particles over rural Hungary. *Atmos. Environ.,* **35,** 4347–4355.

Torres, O., P. K. Bhartia, J. R. Herman, A. Sinyuk, P. Ginoux, and B. Holben, 2002: A long-term record of aerosol optical depth from TOMS observations and comparison to AERONET measurements. *J. Atmos. Sci.,* **59,** 398–413.

Weingartner, E., H. Burtscher, and U. Baltensperger, 1997: Hygroscopic properties of carbon and diesel soot particles. *Atmos. Environ.,* **31,** 2311–2327.

Wolff, G. T., M. S. Ruthkosky, D. P. Stroup, P. E. Korsog, M. A. Ferman, G. J. Wendel, and D. H. Stedman, 1986: Measurements of SOx, NOx and aerosol species on Bermuda. *Atmos. Environ.,* **20,** 1229–1239.

Zappoli, S., and Coauthors, 1999: Inorganic, organic and macromolecular components of fine aerosol in different areas of Europe in relation to their water solubility. *Atmos. Environ.,* **33,** 2733–2743.

Zhang, J., S. A. Christopher, and B. N. Holben, 2001: Intercomparison of smoke aerosol optical thickness derived from GOES 8 imager and ground-based sun photometers. *J. Geophys. Res.,* **106,** 7387–7397.